

Antarctic Bottom Water Flux in the Equatorial Western Atlantic*

MELINDA M. HALL, MICHAEL MCCARTNEY, AND J. A. WHITEHEAD

Woods Hole Oceanographic Institution, Woods Hole, Massachusetts

(Manuscript received 7 October 1996, in final form 18 February 1997)

ABSTRACT

A moored array at the equator in the western basin of the Atlantic provides a 604-day time series of abyssal currents and temperatures spanning the full breadth of the Antarctic Bottom Water (AABW) flowing from the Brazil Basin to the Guiana Basin. Mean AABW transport is estimated to be 2.0 Sv ($\text{Sv} \equiv 10^6 \text{ m}^3 \text{ s}^{-1}$), comprising organized westward flow of 2.24 Sv and return flow of 0.24 Sv. The low-frequency variability is dominated by a quasi-annual transport cycle of amplitude 0.9 Sv and a 120-day period of amplitude 0.6 Sv. Maximum transports occur in September–October, while minimum transports occur in February–March. Allowing for this quasi-annual cycle and extrapolating the 604-day record to a full two years adds about 7% to the estimated mean AABW transport. The array also provides limited sampling in the overlying lower North Atlantic Deep Water (LNADW), where a southern boundary intensified flow of LNADW gives the strongest recorded mean speed through the array, 9.9 cm s^{-1} into the Brazil Basin. The LNADW records also have a quasi-annual cycle with strong LNADW flow episodes occurring in April–May. Time series of temperature indicate that the LNADW/AABW transition layer rises and falls in synchrony with the quasi-annual AABW transport cycle (uplifted transition layer during strong AABW transport periods). An observed overall warming trend appears to be accompanied by a decline in AABW transport.

1. Introduction

The World Ocean Circulation Experiment (WOCE) Deep Basin Experiment (DBE) was conceived as a process study to investigate important aspects of deep and bottom water flow (Hogg et al. 1996). This large internationally coordinated project was designed to observe and quantify the deep and bottom water circulation within an abyssal ocean basin, including making the measurements necessary to provide a bottom water mass balance, distinguishing between boundary and interior mixing processes, understanding how passages affect the flow of water through them, and studying the means by which deep water crosses the equator. The Brazil Basin, Fig. 1a, was chosen as the site for the DBE because the basin geometry and bathymetry are simple, because transport estimates indicate substantial net northward flow of bottom water and net southward flow of deep water through the basin, and because the bathymetry particularly constrains the inflows and outflows of bottom water to small fractions of the basin's boundary thereby making direct measurement practical.

The shoals of the Rio Grande Rise define the sepa-

ration of the Brazil Basin from the immediate source of Antarctic Bottom Water (AABW) in the Argentine Basin to the south. That rise confines the northward flow of AABW to two pathways: to the west, AABW flow is concentrated at the Vema Channel (Hogg et al. 1982) but also extends over the deeper part of the continental slope (Speer and Zenk 1993); to the east, northward transport through the Hunter Channel has been detected (Speer et al. 1992). The combination of these inflows is estimated as 6.7 Sv ($\text{Sv} \equiv 10^6 \text{ m}^3 \text{ s}^{-1}$) (Speer and Zenk 1993). In the north AABW leaves the basin by two routes: eastward through the Romanche Fracture Zone into the eastern Atlantic (Metcalf et al. 1964; Polzin et al. 1996; and Mercier et al. 1994) and northward across the equator into the western North Atlantic (Whitehead and Worthington 1982; McCartney and Curry 1993). Estimates of these combined outflows range from 3 to 6 Sv. In the DBE each of these inflow/outflow sites has been the focus of concentrated measurements, directed to both specific local issues and to the overall goal of constraining the mass balance for AABW within the Brazil Basin during the DBE.

Our involvement in the DBE centers on a current meter array and supportive hydrographic measurements in the flow of AABW from the Brazil Basin into the western North Atlantic. At first glance (Fig. 1a), a direct measurement of AABW flow at the equator seems a tough design problem, for though the Mid-Atlantic Ridge is relatively close to the western boundary at the equator, the exit site is by no means a narrow channel. But the AABW

* Woods Hole Oceanographic Institution Contribution Number 9376.

Corresponding author address: Dr. Melinda M. Hall, Department of Physical Oceanography, Woods Hole Oceanographic Institution, Woods Hole, MA 02543.

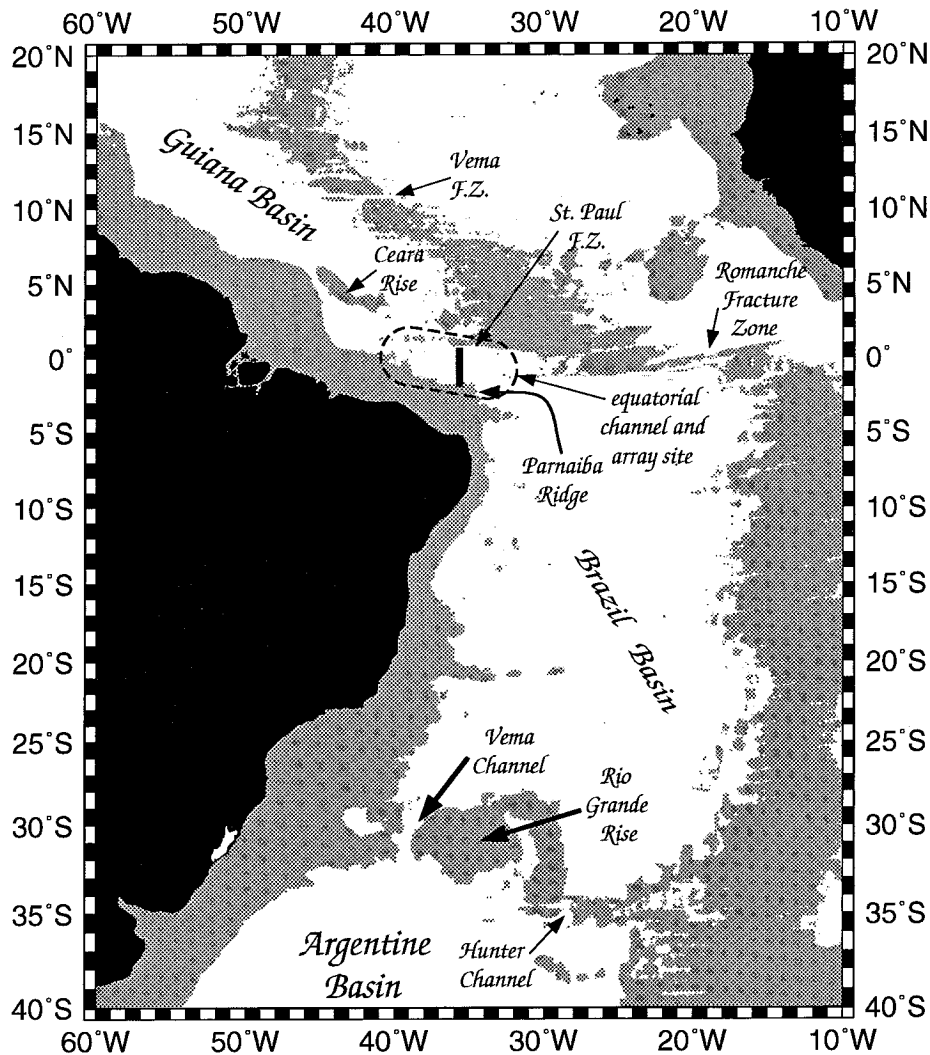


FIG. 1a. Setting for northward flow of Antarctic Bottom Water through the western basin. The principal basins and channel connecting them, some blocking rises, and two fracture zones that allow eastward abyssal flow through the Mid-Atlantic Ridge all are delineated by the shading for depths less than 4000 m (bathymetry from the "Etopo5" database, National Geophysical Data Center 1988). The oval indicates the confined passage for cross-equatorial flow from the Brazil Basin to the Guiana Basin, with the meridional bar denoting the moored array across that passage; details are shown in Fig. 1c.

is a fairly thin layer at the equator (Fig. 1b), and artifacts of the regional bathymetry confine it to a zonally oriented channel-like passage of only about 300-km width. Specifically, the Parnaiba Ridge projects eastward from the western boundary near 1°S, with its crest between 3500 and 4000 m, defining the southern channel wall, and the westward extension from the Mid-Atlantic Ridge of the St. Paul Fracture Zone defines the north wall, also cresting above 4000 m (Fig. 1c). The abyssal channel (with depth ~4500 m) is aligned along the equator, and AABW from the Brazil Basin to the south enters the eastern end of the channel from eastward of the terminus of the Parnaiba Ridge. The AABW is constrained by the channel to flow westward along the equator and exits northward from the channel westward of 38°–40°W, the terminus of the St.

Paul Fracture Zone. Thereafter, it flows over the Ceara Abyssal Plain and begins its northward descent into the Guiana Basin at about 4°N.

In addition to providing an estimate of the outflow from the Brazil Basin, the equatorial moored array provides an estimate of the inflow to the Guiana Basin. Earlier estimates ranged from 1–4 Sv: More accurate quantification of the AABW transport is important for quantifying the meridional overturning cell of the North Atlantic, as AABW is a major contributor to the lower North Atlantic Deep Water (LNADW), which dominates the cold water export from the North Atlantic by this cell (Luyten et al. 1993).

The moored array design was based on the property fields associated with the 1983 and 1987 sections near

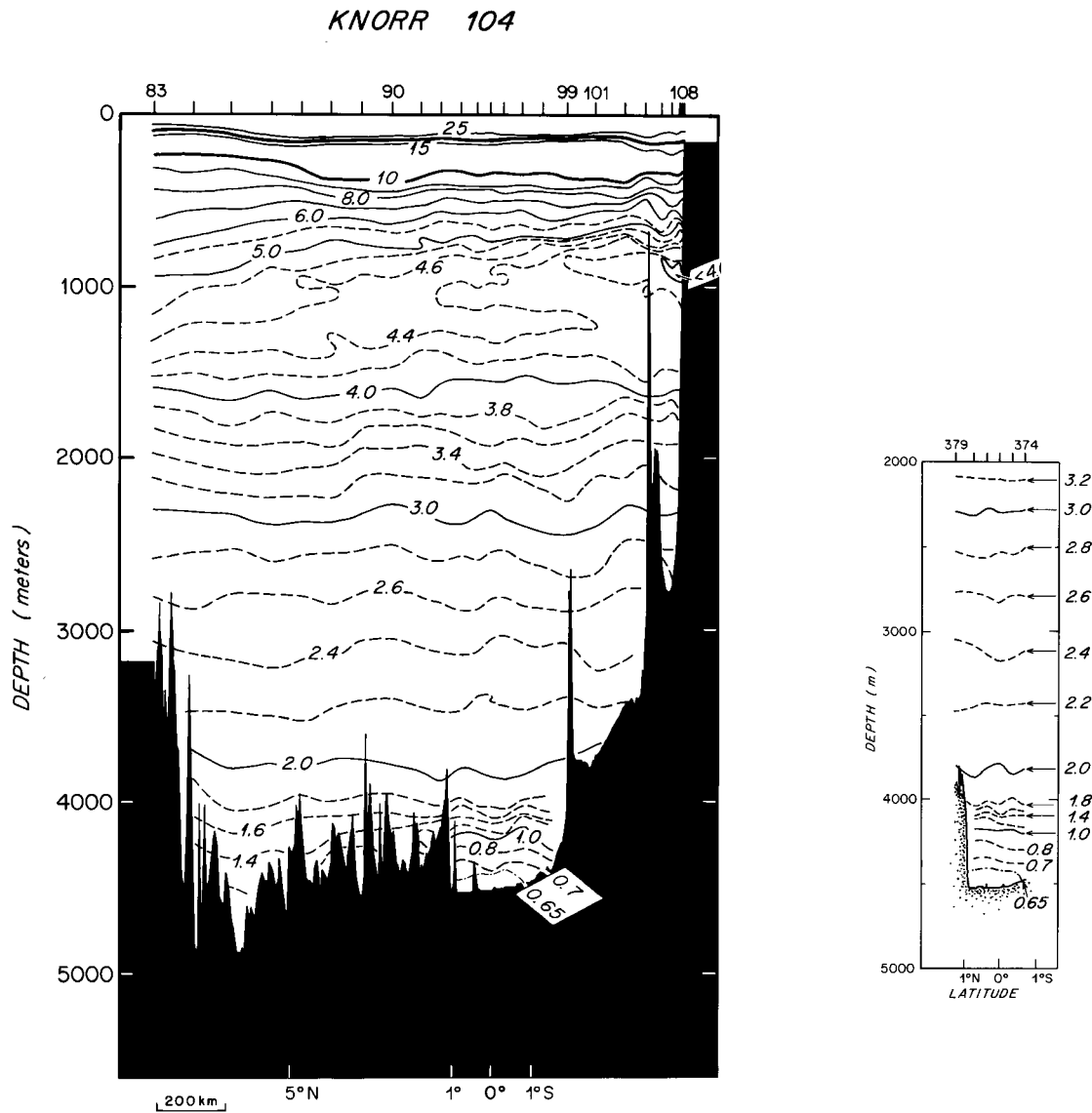


FIG. 1b. Potential temperature sections across the abyssal equatorial passage that channels the cross-equatorial flow of Antarctic Bottom Water into a westward flow along the equator. From McCartney and Curry (1993), data taken in 1983 (left) and 1989 (right), locations about 50–100 km west of the moored current meter array, Fig. 1c.

37°W (Fig. 1b). We took advantage of the narrowness of the equatorial channel and the thinness of the AABW layer to rather densely instrument the AABW, but velocity was also measured in the overlying LNADW to explore its transport distribution and to measure the shear between LNADW and AABW for comparison to geostrophic shear estimates near and at the equator. Mooring positions are included on Fig. 1c, and Table 1 summarizes deployment and recovery statistics and data returns; the instruments worked well and together provide a roughly 20-month-long sampling of the AABW and adjacent flow elements. In section 2 the moored measurements of velocity and temperature are described, as well as the hydrographic sections collected at three times: during deployment, about one month

before recovery, and during recovery. Section 3 presents the methodology for calculating time series of AABW transport through the array and describes the results of these calculations. Section 4 discusses the results in the context of western basin deep circulation, and also notes some evidence for long-term evolution of the AABW distribution at the equator. Section 5 summarizes the main results.

2. The experiment: Hydrography and moored array results

a. Experimental design and data return

In October 1992, six moorings were deployed from the R/V *Iselin* near 36°W on a meridional line from

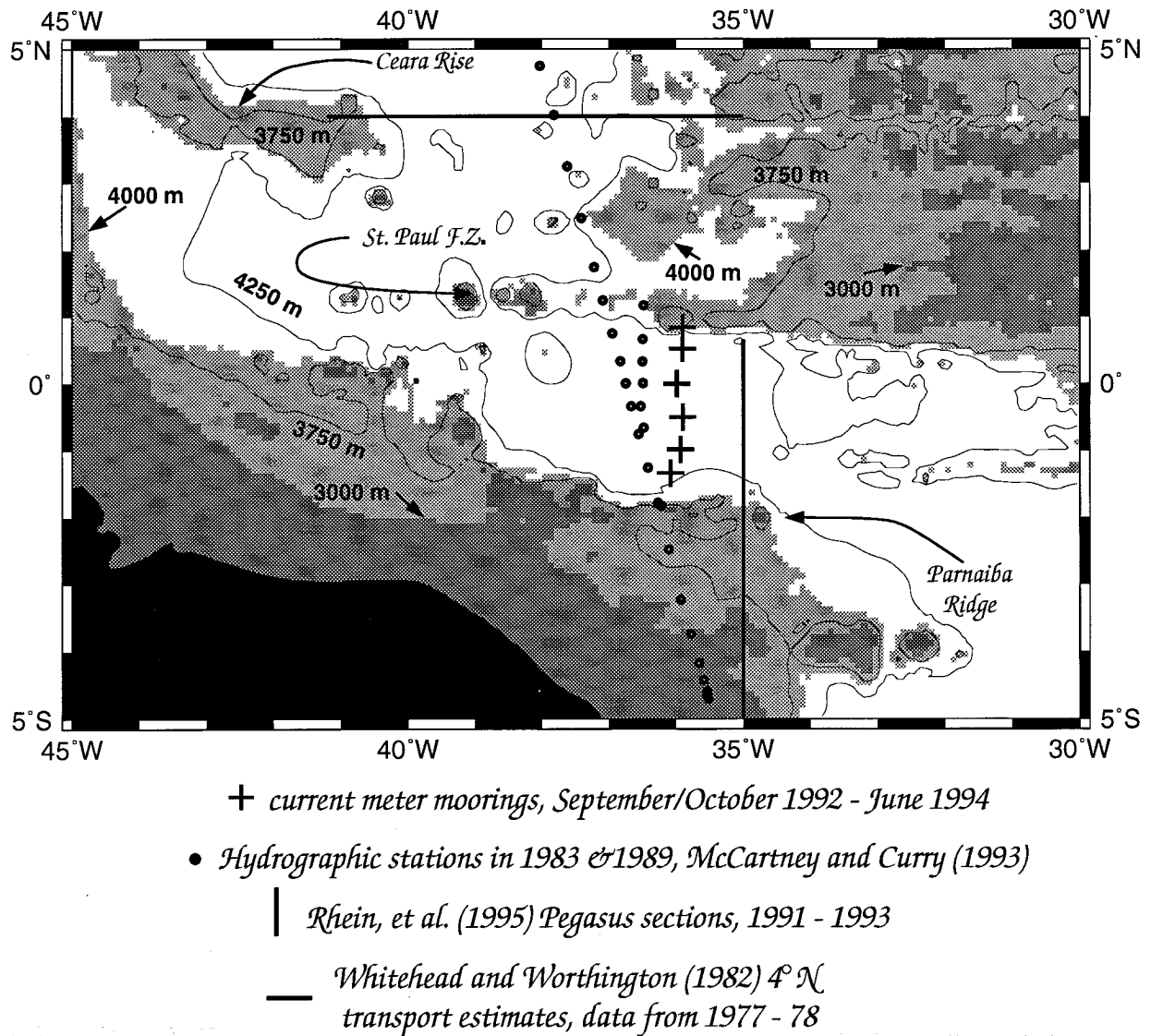


FIG. 1c. Detailed setting of the equatorial passage (bathymetry from the "Etopo5" database; National Geophysical Data Center 1988), showing the placement of the six moorings of this experiment (Table 1) and locations of other data and earlier experiments. We refer to the moorings with numbers 1 (southern most) through 6 (northernmost).

TABLE 1. Current meter mooring durations and locations. For clarity, the moorings are referred to with numbers 1-6, 1 being the southernmost and 6 the northernmost.

Mooring number	WHOI mooring number	Date set	Date received	Latitude	Longitude	Bottom depth (m)
6	936	28 Sep 1992	2 Jun 1994	00°50.16'N	35°54.02'W	4486
5	937	28 Sep 1992	1 Jun 1994	00°30.10'N	35°54.17'W	4539
4	938	29 Sep 1992	1 Jun 1994	00°00.28'S	35°59.46'W	4536
3	939	30 Sep 1992	31 May 1994	00°30.05'S	35°54.06'W	4485
2	940	1 Oct 1992	31 May 1994	00°58.80'S	35°55.95'W	4396
1	941	2 Oct 1992	3 Jun 1994	01°19.90'S	36°04.94'W	4450

1.0°N to 1.5°S, which was a location about 1° east of the sections shown on Fig. 1b. Figure 2 shows the moored instrument placements (Table 1) superimposed on sections of potential temperature acquired during deployment and recovery cruises. In the hydrographic data available during the design phase (Fig. 1b), the coldest observed AABW was twice found right on the equator, and one realization of the temperature distribution exhibited an abyssal concavity suggestive of the equatorial geostrophic expression of a westward flow along the channel centered on the equator. But rather than tuning the array design to an equatorially aligned flow, we opted for even sampling across the breadth of the channel, resulting in a mooring spacing of 30 n mi. This was thought to be an array closely spaced enough to ensure sampling the AABW flow wherever in the channel it might be found—provided the flow filaments were not too narrow. Spanning the full channel turned out to be prudent, for the observed AABW flow was concentrated south of the equator: that is, it retains its character as a western boundary current even at these low latitudes. The spacing of 30 n mi turns out to be marginal for resolving the horizontal distribution of AABW flow.

On all the moorings we placed instruments at three common nominal levels, 3900, 4100, and 4300 m (potential temperature $\theta \approx 1.94^\circ$, 1.43° , and 0.79°C , respectively), to obtain measurements in the AABW, the overlying LNADW, and the transition layer in-between. Because mean flow at the middle level is primarily westward (and $\theta \lesssim 1.5^\circ\text{C}$), we also refer to water at this level as the warmer AABW. At the time of the array design, ongoing work suggested that while the AABW flow would be westward in the channel, flow in the LNADW would reverse to eastward, at least in the southern part of the channel (McCartney 1993; Friedrichs et al. 1994). The selection of these three levels was to measure the absolute velocity field of this layered and vertically sheared flow. Additional instruments were placed on the equatorial mooring: near the bottom (4485 m, $\theta \approx 0.6^\circ\text{C}$), to measure the AABW flow more completely should the velocity maximum be there; and at three additional levels in the LNADW, 3600, 3300, and 3000 m ($\theta \approx 2.1^\circ$, 2.2° , and 2.4°C), to explore the velocity associated with thin layered LNADW structure (McCartney 1993). For additional guidance regarding the LNADW circulation and geostrophic reference level issues, the 1°N and 1°S moorings were instrumented at 3300 m ($\theta \approx 2.2^\circ\text{C}$). All of these 24 instruments were vector averaging current meters (VACMs) provided by the subsurface mooring operations group at the Woods Hole Oceanographic Institution. F. Schott of IFM Kiel added to the array four Aanderaa current meters at nominal depths 1900, 1700, 1500, and 1300 m ($\theta \approx 3.5^\circ$, 3.9° , 4.1° , and 4.3°C) on the equatorial mooring for exploration of the deep equatorial jets of this region (Ponte et al. 1990); these shallow data are described by Fischer and Schott (1997).

The moorings were launched from the R/V *Iselin* in

September–October 1992, accompanied by a conductivity–temperature–depth (CTD) section. Three changes occurred to planned mooring positions at the time of deployment. The equatorial mooring ended up 5 miles west of the planned site due to a swift surface current affecting the deployment. The mooring at 1°S was moved slightly due to a bump in the sea floor, with the location chosen such that the instruments would be at the same depths as those on the other moorings. Finally, the southernmost mooring was repositioned to be outside Brazilian waters, as the government of Brazil did not grant clearance to deploy within their waters. After approximately 20 months, in June 1994, the moorings were recovered on a cruise aboard the R/V *Knorr* and another CTD section was made. For both sections, stations were made at and between mooring locations, for a total of 11 stations each time. In addition, an extensive DBE hydrographic cruise was made from the R/V *Knorr* preceding our recovery cruise, and Bill Smethie included in that work a third CTD section along the mooring line, this one with a full suite of tracer measurements, completed about 30 days before our recovery work. The details of the deployment and recovery sections are summarized in Table 2.

The data return from the VACMs (Table 3) was remarkable: with two exceptions each instrument collected over 600 days of continuous time series of $u(t)$, $v(t)$, and $T(t)$. On the 3300-m instrument at 1°S the vane stuck after 262 days but, since that is well above the top of the bottom water, it does not hamper the transport calculations. The other data loss was a 10-day gap in the middle of the 4300-m velocities and temperature at the southernmost mooring. For the purposes of this investigation, we have linearly interpolated the three time series through the gap, starting with the low-passed daily subsampled time series that have been used in all the calculations. Additional details regarding the data may be found in Tarbell et al. (1997). Time series plots of vector velocity and temperature for the three primary sampling levels are shown in Fig. 3. In the vector plots, east is up.

The velocity time series recorded at the 1°S mooring at 4300 m differs in character from time series to the north and south (Fig. 3c). The mean speed is low compared to means at the 4300-m level at 0.5°S and 1.5°S (Rhein et al. 1995; Rhein et al. 1996) and seemingly inconsistent with the strong deep shear implied by the thermal wind balance at this longitude during Smethie's hydrographic section, Fig. 2b (at 1°S). But the only anomaly found in the instrument records is a note that the instrument had an overheated electronics odor on opening after recovery. The peculiar character of the speed record was not noted until after the instrument was redeployed for another experiment, so it has not been reexamined. Recall, however, that this instrument was in the wake of an abyssal shoal: as sited, this mooring still was on the edge of this feature, and the bottom current meter is closer to the sea floor than the bottom

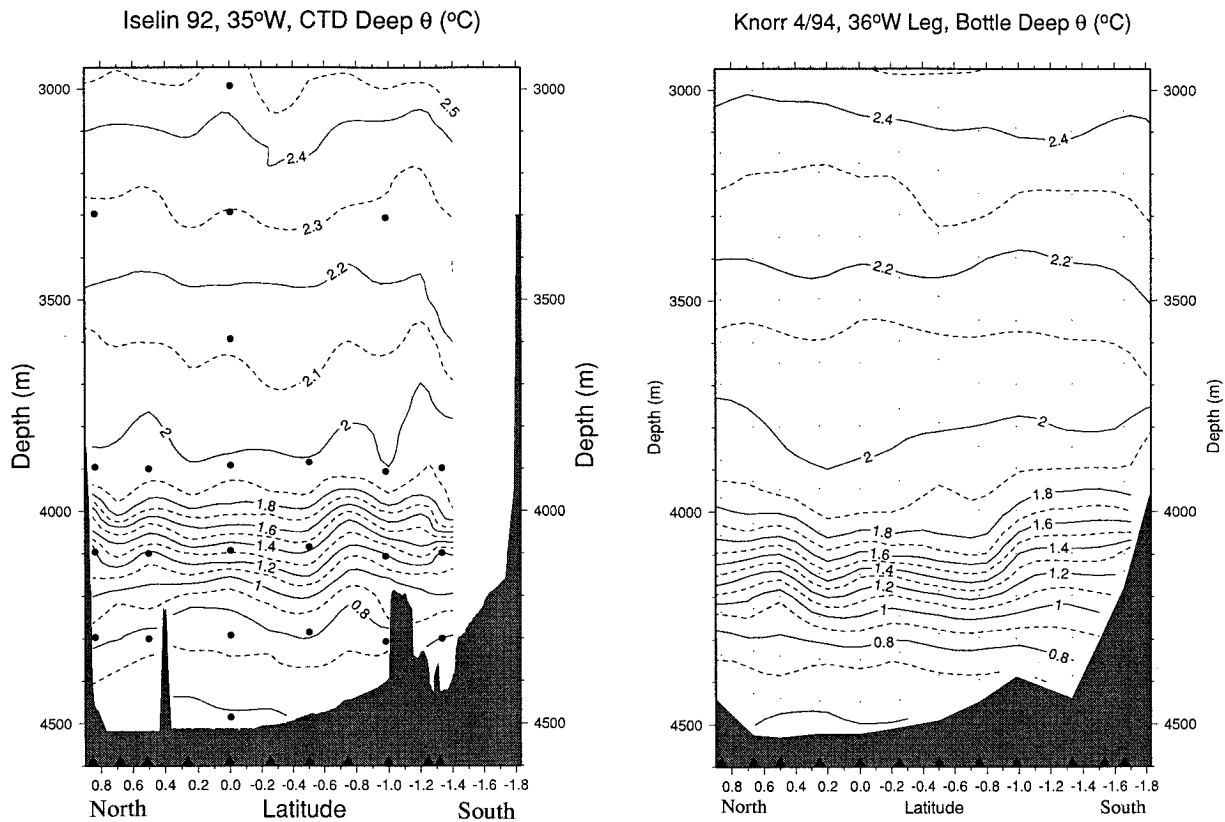


FIG. 2. Deep potential temperature for three hydrographic sections near the location line of the moored array. Dots show the moored instruments, and triangles along the abscissa show the station locations for the contoured temperature field.

instruments at the adjacent moorings. We have retained this record in our analysis and will comment briefly later on how this record might affect our overall AABW transport estimate.

b. Mean currents in the abyssal equatorial channel

As a first look at the data, Fig. 4a shows the record-mean current vectors superimposed on a map of the bathymetry around the equatorial array. Moorings will be referred to by numbers 1–6 with 1 being the southernmost and 6 the northernmost. Maps are shown for each of the three primary sampling levels. The strong flows are confined to the south of the equator, as anticipated for the LNADW, but not as anticipated for the AABW. However, the southern intensification pattern observed at the 3900-m and 4300-m levels is similar to the three Pegasus current profile snapshots 1° east of our array by Rhein et al. (1995), one taken in late October 1992 while our array was in the water. As expected, Fig. 4a shows net westward flow of AABW at the deepest level and net eastward flow of LNADW at the shallowest level. At the level in between, which can be considered the transition layer from AABW to LNADW, there is also a net westward flow, with eastward mean flow only at the southernmost instrument.

This vertical shear (eastward speed decreasing downward or equivalently westward speed increasing downward) is consistent with thermal wind and a southward rise of the transition layer between LNADW and AABW south of the equator, as shown in Figs. 2b and 2c. At 0.5° and 1.0° S, speeds in the 4100-m layer are slightly larger than at the deepest level, indicative of a slight shear reversal near the bottom of the transition layer.

At the 3900-m LNADW level (Fig. 4a, top panel), the impression is that of a southern boundary layer with maximum eastward speeds at the southern mooring, which decrease by 45% 30 n mi to the north, then change to northwestward flow between there and 60 n mi, and to northward flow on the equator at mooring 4. With the 3900-m contour of the Parnaiba Ridge falling about 24 n mi south of mooring 1, this eastward flowing boundary layer of LNADW appears to be about 80–90 n mi wide. The net transport at 3900 m across the 4 northern moorings is westward and about 15% the size of the eastward transport in the southern boundary layer. This may reflect a degree of recirculation of LNADW, which is a partial retroflection of the eastward flow in the southern boundary layer. This has been inferred from hydrographic measurements (McCartney 1993, Friedrichs et al. 1994) but was not conclusively evident from a few Pegasus measurements (Rhein et al.

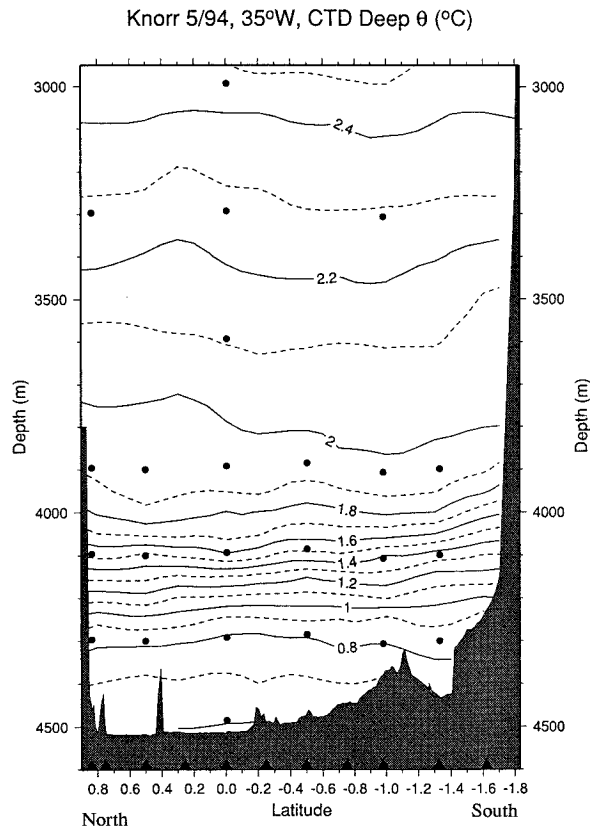


FIG. 2. (Continued)

1995). At the 4100-m level (Fig. 4a, middle panel), there is much weaker eastward flow in the south that gives way to a westward flowing jet centered south of the equator. At the two northern moorings, mean flow is weak. At the AABW level (4300 m; Fig. 4a, lower panel) westward flow is found at all three of the moorings south of the equator as well as at the mooring on the equator. Because of the low mean speed at mooring 2, the westward flow amplitude varies across the southern part of the array. North of the equator, amplitude is very small.

In summary, the mean fields show the southward intensified eastward flow of LNADW in a southern boundary layer, with a footprint extending down into the transition layer at the southernmost mooring. There is a transition to distinct westward flow north of the southern boundary layer in both the LNADW and the transition layers. The westward AABW flow appears to be broad, but mostly south of the equator. At all three depths, mean flows at the two northern moorings are weak.

c. Time variability of the currents in the abyssal equatorial channel

Next we consider aspects of the time variability in the moored records. How well defined are the mean velocity vectors and the temperatures? Figure 5 shows

TABLE 2. CTD stations occupied during the deployment and recovery cruises.

Station	Latitude	Longitude	Date 1992	Moor- ing	Station depth (m)
4	0°51.14'N	35°53.86'W	28 Sep	6	4463
5	0°30.72'N	35°54.39'W	28 Sep	5	4525
6	0°41.04'N	35°52.79'W	29 Sep		4523
7	0°0.34'N	35°54.24'W	29 Sep	4	4525
8	0°15.84'N	35°54.58'W	30 Sep		4527
9	0°15.03'S	35°53.79'W	30 Sep		4515
10	0°30.08'S	35°55.13'W	30 Sep	3	4490
11	0°44.74'S	35°54.59'W	30 Sep		4463
12	0°59.82'S	35°53.51'W	1 Oct	2	4281
13	1°14.77'S	35°54.42'W	1 Oct		4424
14	1°19.14'S	36°4.32'W	1 Oct 1994	1	4441
1	1°37.28'S	36°02.33'W	30 May		4205
2	1°19.57'S	36°55.29'W	31 May	1	4439
3	0°58.81'S	35°55.96'W	31 May	2	4381
4	0°29.91'S	35°53.95'W	31 May	3	4470
5	0°14.86'S	35°59.70'W	1 Jun		4494
6	0°0.02'W	35°55.17'W	1 Jun	4	4517
7	0°15.29'N	35°59.75'W	1 Jun		4519
8	0°29.94'N	35°54.17'W	1 Jun	5	4525
9	0°45.17'N	35°59.54'W	2 Jun		4519
10	0°50.26'N	35°50.62'W	2 Jun	6	4468
11	0°44.93'S	35°54.06'W	2 Jun		4451

progressive vector diagrams for each of the three primary sampling levels, plotted to maximize the displacement scale. At locations where the magnitude of the mean velocity exceeds 4 cm s^{-1} , mean kinetic energy (K_M) exceeds eddy kinetic energy (K_E) (Table 3), and the corresponding progressive vector diagrams show a quasi-steady situation where displacement accumulates rather steadily in one general direction with small veering. In fact, this is the case for roughly half the instruments, even where $K_E > K_M$. In the northern half of the array, however, mean flows are weak and are dominated by eddies (moorings 5 and 6 in Fig. 5).

Like most moored records around the world, our data have considerable variability over a broad range of periods (Figs. 3a–c). When low-pass filtered (40 days) to suppress the higher frequencies, a quasi-annual signal is the strongest signal, with strong AABW speeds in September–October and weak AABW speeds in February–March. The LNADW flow in the south tends toward the reverse cycle, but with its strongest eastward flow peaking somewhat later than the minimum westward AABW flow. Figures 4b,c,d show the mean vectors at these times during strong westward AABW flow (at the beginning of the experiment and a year later); during weak westward AABW flow (about six months into the experiment and a year later), and during strong eastward LNADW flow (about seven months into the experiment and a year later). Here we describe the field of current vectors during these three distinct flow regimes. The implications of the quasi-annual signals for AABW transport are discussed in section 3.

TABLE 3. Statistics of the current meter records. The southernmost mooring is number 1 and the northernmost is 6. Overbars denote a record-length mean. K_M is mean kinetic energy, $(\bar{u}^2 + \bar{v}^2)/2$; K_E is eddy kinetic energy, $(\overline{u'^2} + \overline{v'^2})/2$.

Mooring number	Depth (m)	\bar{u} (cm s ⁻¹)	\bar{v} (cm s ⁻¹)	T (°C)	$\overline{u'^2}$ (cm ² s ⁻²)	$\overline{v'^2}$ (cm ² s ⁻²)	$(\overline{T'^2})^{1/2}$ (°C)	$\overline{u'v'}$ (cm s ⁻¹)	K_M (cm ² s ⁻²)	K_E (cm ² s ⁻²)
6	3297	-1.14	-0.86	2.547	10.60	11.69	0.0186	2.86	1.01	11.14
	3896	0.75	0.46	2.278	8.84	3.77	0.0282	2.75	0.39	6.30
	4096	-0.12	-0.05	1.812	4.14	1.39	0.1266	-0.73	0.01	2.77
	4297	0.35	0.07	1.135	2.65	0.71	0.0446	-0.04	0.06	1.68
5	3900	-0.40	0.89	2.280	12.56	7.96	0.0232	6.01	0.48	10.26
	4100	-0.13	-0.11	1.769	8.92	4.03	0.1344	2.16	0.01	6.48
	4300	0.02	0.14	1.116	6.65	3.23	0.0390	2.70	0.01	4.94
4	2993	-0.93	-0.31	2.724	12.26	9.65	0.0275	0.60	0.48	10.96
	3293	-2.02	0.15	2.557	9.40	6.42	0.0223	-0.68	2.05	7.91
	3593	-2.12	0.27	2.432	9.34	2.74	0.0245	-0.11	2.27	6.04
	3892	-0.22	2.41	2.292	4.69	5.89	0.0257	1.96	2.93	5.29
	4093	-1.78	0.46	1.800	6.05	3.37	0.1356	-1.74	1.68	4.71
	4292	-0.64	0.04	1.126	5.49	2.53	0.0363	-1.50	0.21	4.01
	4485	-1.31	0.46	0.929	3.16	1.99	0.0128	-0.29	0.96	2.57
3	3885	-1.54	1.56	2.303	9.28	7.30	0.0187	1.40	2.39	8.29
	4085	-5.53	0.72	1.851	24.86	4.54	0.1268	0.17	15.55	14.69
	4285	-4.22	0.32	1.147	10.97	2.73	0.0409	-1.16	8.96	6.84
2	3307	1.33	0.28	2.535	4.02	2.48	0.0186	0.81	0.92	3.25
	3907	5.39	0.89	2.278	25.49	7.76	0.0235	6.30	14.92	16.63
	4107	-1.91	0.98	1.669	13.74	12.14	0.1029	4.83	2.30	12.94
	4307	-1.35	0.02	1.124	6.92	8.50	0.0353	4.41	0.91	7.71
1	3899	9.90	-0.65	2.247	19.75	6.68	0.0455	1.97	49.17	13.22
	4099	1.48	0.86	1.685	8.43	6.84	0.1115	2.73	1.46	7.63
	4300	-4.88	-0.42	1.192	12.70	2.50	0.0367	2.38	12.00	7.60

During the two periods of strong westward AABW transport, the vectors at moorings 1, 2, and 3 that dominate the flow at 4300 m are 20% to 50% greater than the record means (Figs. 3c and 4b, bottom panel). At the transitional level of 4100 m, the flow is more divergent during the strong westward AABW transport periods than on average (Fig. 4b, middle panel). In particular, westward velocities at moorings 2 and 3 have accelerated by about 70%, but at mooring 4, on the equator, the velocity is nearly northward, rather than its record-average direction of nearly due westward, though with little change of speed. This northward flow appears to turn east at mooring 5, north of the equator, where a modest eastward flow develops. At mooring 1, south of the westward jet, the eastward flow observed in the mean is intensified during the two periods of strong westward AABW transport (Fig. 4b, middle panel). In contrast, the eastward flow of the southern boundary layer in the overlying LNADW at 3900 m is substantially reduced at moorings 1 and 2 (Fig. 4b, top panel), while net westward transport across moorings 3–6 increases and is 45% as large as the southern eastward flow. In summary, during the two periods of strong westward AABW transport, the westward flow of both colder AABW (4300 m) and warmer AABW in the transition layer (4100 m) is greater; but at 4100 m, the eastward recirculation in the south has actually strengthened, and weak eastward flow has also developed north of the equator. The eastward flow of LNADW in the southern boundary layer (moorings 1 and 2) is slower when the

westward transport of AABW is strong, but north of the boundary layer the northwestward and northward flows of LNADW are little changed.

The two periods of weak westward AABW flow show a greatly diminished flow amplitude at 4300 m (Fig. 4c, bottom panel), in the colder part of the AABW. At 4100 m, in the warmer part of the AABW (Fig. 4c, middle panel), the westward jet present at moorings 2, 3, and 4 in the mean field has diminished greatly. At the same time, the eastward flow in the southern boundary layer has broadened to mooring 2 and has strengthened relative to the mean situation. This southern recirculation of warmer AABW is twice as large the weakened westward flow at moorings 3 and 4. At 3900 m during this period of weaker AABW flow at depth, the eastward flow of LNADW in the southern boundary layer has accelerated (Fig. 4c, top panel), and the net flow of LNADW offshore reverses to weakly eastward, with distinct northward LNADW flow at moorings 3, 4, and 5.

Shortly after the two periods of weakest westward AABW flow are two periods of strongest eastward flow of LNADW (Figs. 3a,b,c). Accompanying the pronounced acceleration of eastward speeds at 3900 m (Fig. 4d, top panel) at the southern two moorings, there is an enhancement at the next two moorings to the northward flow that exists to some degree in all these 3900-m vector plots. However, net transport is again very weakly eastward. The two periods of strong LNADW transport in the southern boundary layer at 3900 m exhibit pattern shifts in the flows at the other two levels. At

4100 m (Fig. 4d, middle panel), the warmer AABW in the transition layer still shows a jetlike structure, but the jet's center is displaced northward, from mooring 3 to mooring 4 on the equator. Curiously, the eastward recirculation of warmer AABW (4100 m) at the southernmost mooring is weaker in the strong LNADW transport periods than in the record mean and the other periods illustrated in Fig. 4. At 4300 m (Fig. 4d, lower panel), the westward flow of AABW slows down somewhat at moorings 1, 2, and 3, and expands northward to include moorings 4 and 5 at and north of the equator. Thus, the two periods of strong eastward flow of LNADW in the southern boundary layer are characterized by an enhanced northward LNADW flow outside that boundary layer, a northward displacement of the centroid of westward flow of AABW at 4100 and 4300 m, and a near disappearance of warmer AABW recirculation southward of the displaced AABW jet at 4100 m.

d. The deep temperature field

On both the deployment and recovery cruises, CTD sections were occupied across the array, with stations nominally at and between mooring locations, for a total of 11 stations in each section. An additional section was made a few weeks before recovery. Twenty-four water samples were collected at each station and analyzed for salinity to calibrate the conductivity sensor. The estimated accuracy of the data is $\pm 0.001^\circ\text{C}$ for temperature and ± 0.003 psu for salinity.

Figure 2 shows θ below 3000 m for all three sections. The 1.8°C potential isotherm is at the top of the strongly stratified transition layer between cold AABW and somewhat warmer LNADW, both of which are more weakly stratified. This layer of stronger vertical density gradient is extensive in the tropical and subtropical North and South Atlantic. At extra-equatorial locations, it is the tilt of this transition layer that dominates the geostrophic shear between the two water masses and, with suitable reference level inference, was used by Wright (1970) to produce the first comprehensive treatment of the western basin AABW transport distribution. While direct usage of geostrophy within 1.5° latitude of the equator is a delicate matter, which will not be explored here, note that the current vector plots of Figs. 3 and 4 do show considerable shear across this layer, especially at the southern mooring between the pronounced eastward LNADW flow at 3900 m and the pronounced westward AABW flow at 4300 m. In the 604-day mean there is nearly a 15 cm s^{-1} difference across 400 m. Vertical movement of this transition layer leads to stronger temperature variability at 4100 m, where vertical temperature gradients are relatively high, compared to the variability at 3900 and 4300 m (Table 3). This is illustrated in Fig. 6, which shows time series of T at the seven depths on the equatorial mooring. (From deep pressure measurements, we estimate that the effect of mooring motion on temperature measure-

ments is more than an order of magnitude smaller than the natural variability.) This figure also suggests that there is a long-term warming at 4100 m over the 20-month deployment as well as the same quasi-annual cycle observed in the velocities. In fact, though not discernible by eye in Fig. 6, similar (but weaker) features also occur at 4300 m. Both trends occur at these levels throughout the array. Thermistors at and below the 4100-m level have a 10-yr calibration history, with average drifts of 0.1 to 0.7 millidegrees per year. In contrast, least squares linear fits to the warming trends, after removing the seasonal signal, yield warming rates on the order of 0.098°C/yr at 4100 m, and 0.016°C/yr at 4300 m, about two orders of magnitude greater than the sensor drift rates. The difference in magnitude of the trends at the two depths (about 6 to 1) is the same order as the difference in strength of the vertical temperature gradient at the two levels (about 4 to 1); hence, the warming may also be interpreted as a deepening of the interface between LNADW and AABW. From the beginning to the end of the experiment, this deepening would be about 40 m at 4100 m and 25 m at 4300 m.

Differences in the deployment and recovery hydrographic sections are consistent with the observed temperature variability measured by the VACMs. The recovery section (Fig. 2c) was made during the warm phase of the seasonal cycle: notice that the pool of water colder than 0.6°C is smaller in May 1994 than in October 1992. Long-term variability is discussed in greater detail in section 4. The coldest measured potential temperature also warmed from 0.582°C at $0^\circ 15' \text{S}$ in 1992 to 0.595°C on the equator in 1994. Figure 7 shows the average vertical θ profiles for 1992 and 1994. In 1994, the vertical potential temperature profile below 2°C has descended about 80 m and also flattened out from the somewhat curved nature of the 1992 profile (Fig. 7). The descent is larger than that estimated for the long-term trend alone because the peak-to-peak amplitude of the seasonal cycle is roughly the same size as the trend. In order to facilitate the transport calculations for AABW in section 3, the average temperature gradients $d\theta/dz$ have been calculated from least squares linear fits to the high gradient portions of the $\theta(z)$ curves in Fig. 7. These slopes are $-4.03 \times 10^{-3}^\circ\text{C m}^{-1}$ in 1992 (evaluated over a depth range of 3950 to 4200 m) and $-3.56 \times 10^{-3}^\circ\text{C m}^{-1}$ in 1994 (over 3950 to 4275 m). We have converted the temperature time series to potential temperature using the mean pressure of each instrument and the CTD data as a guide to the departure of the likely actual salinity from a mean value. The method is described in appendix A.

3. Transport calculation

As noted in the introduction, a primary purpose of the current meter deployment was to obtain an accurate measurement of AABW flow leaving the Brazil Basin through this passage. First we had to choose a definition

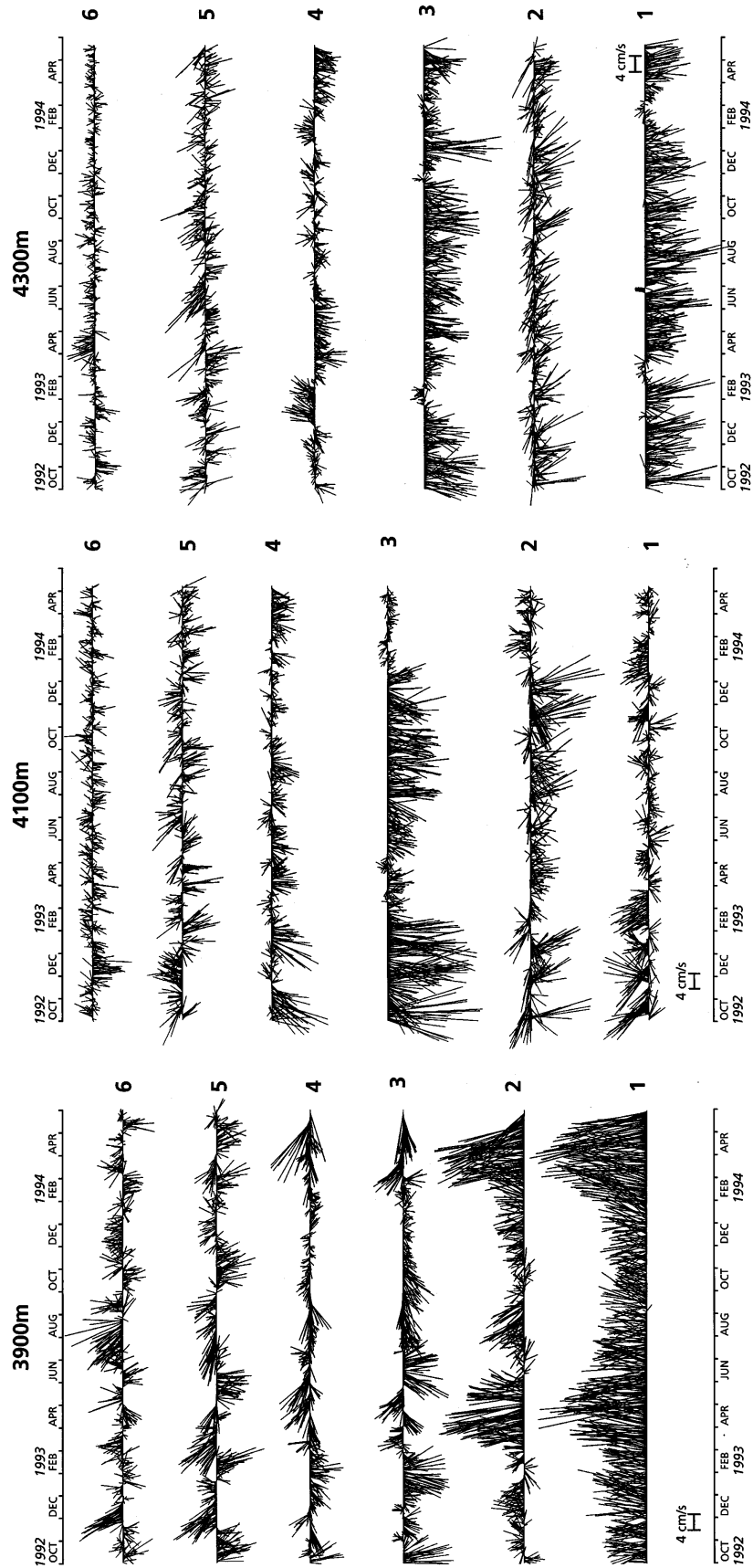


FIG. 3. Time series of daily average vector current and in situ temperatures at the three primary moored array sampling levels. In (a)–(c), east is up. (a) Velocity at 3900 m. (b) Velocity at 4100 m. (c) Velocity at 4300 m. (d) In situ temperature at 3900 m. (e) In situ temperature at 4100 m. (f) In situ temperature at 4300 m.

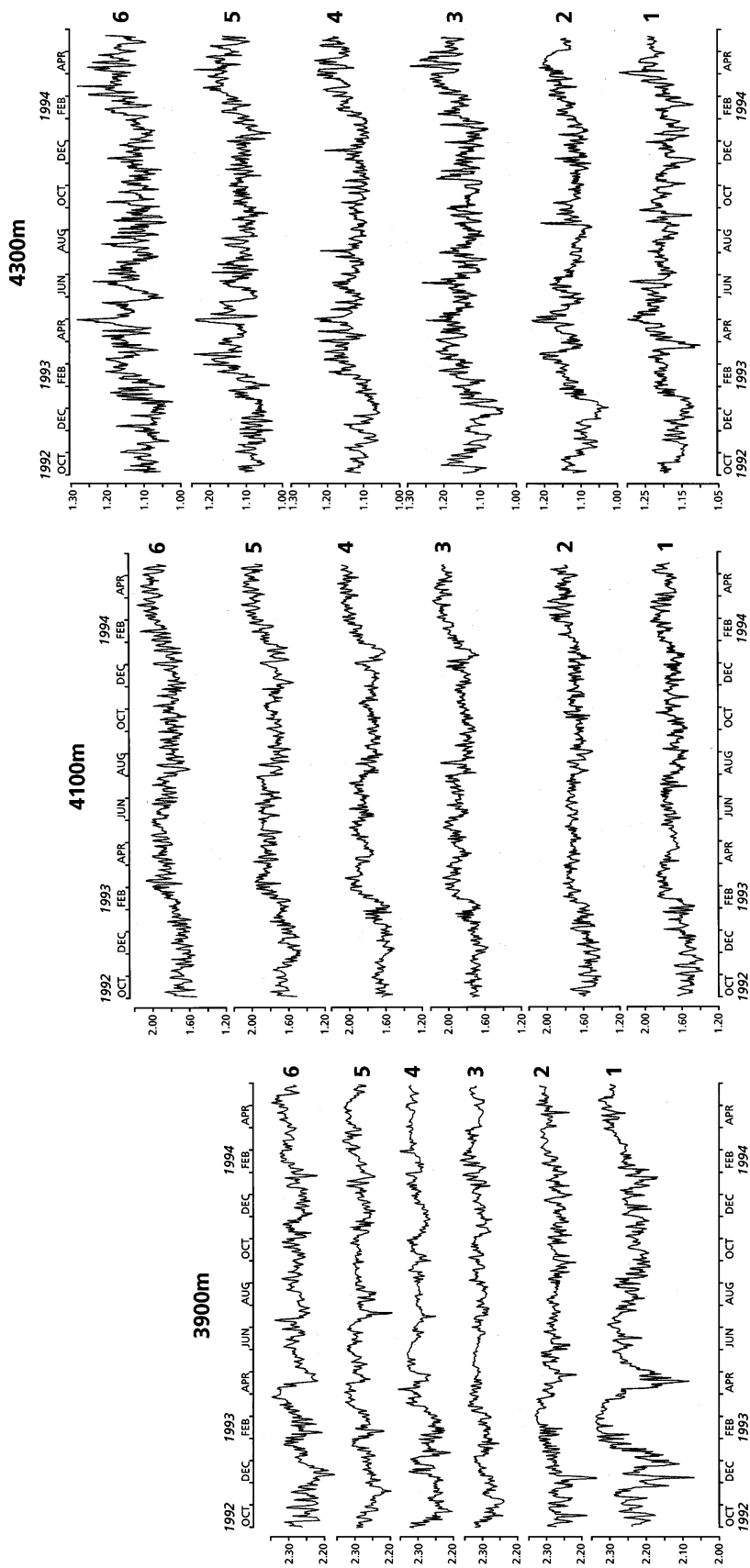


FIG. 3. (Continued)

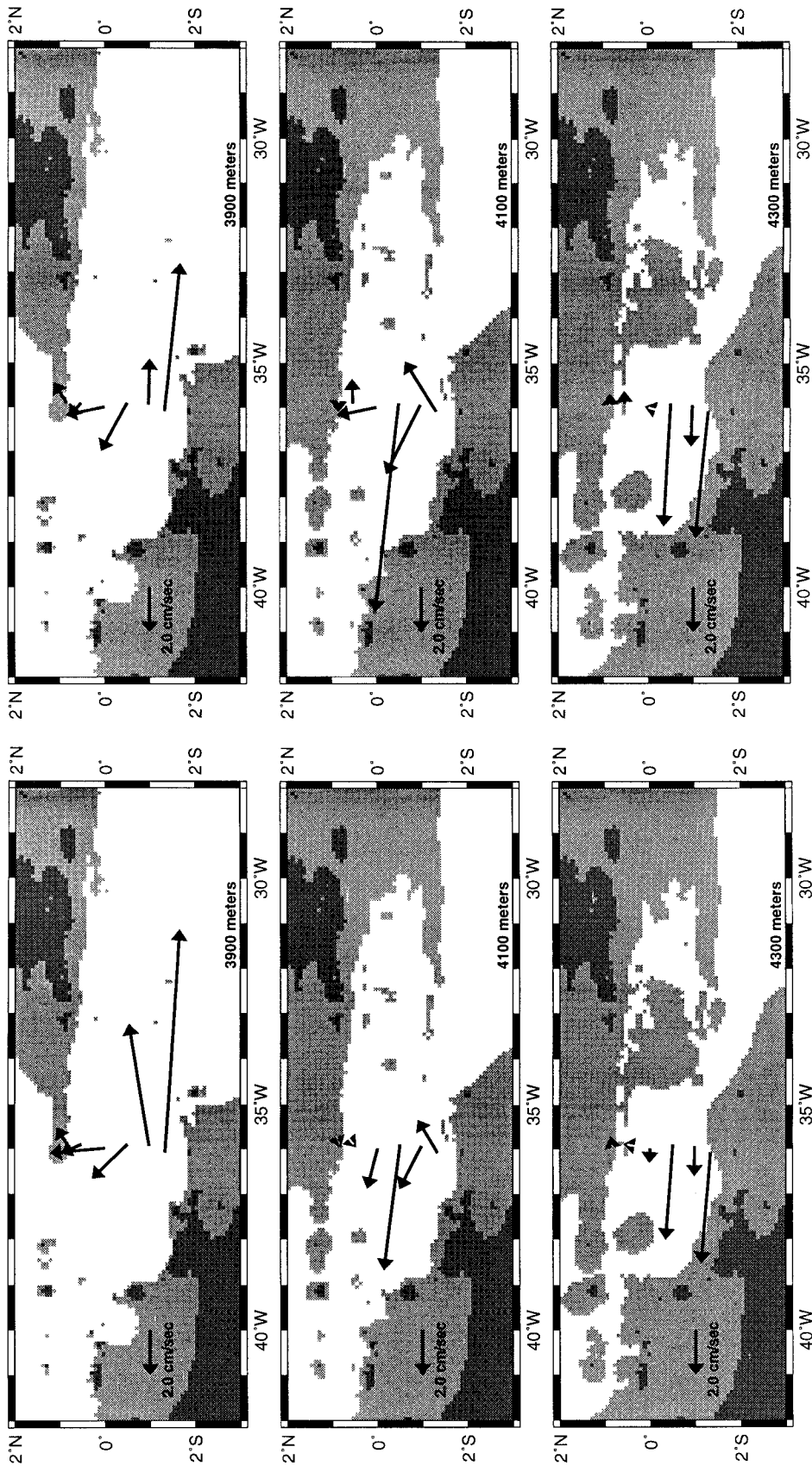


FIG. 4. Mean velocity vectors for the three primary instrumented levels of the moored array. These vectors are projected onto the regional bathymetry: 3000 m is shown on all three images, and the lighter shading on each image is the area where depths are shallower than the nominal depth of those vectors, for example, the 3900-m instruments have the <3900-m depth areas shaded (bathymetry from the "Etopo5" database; National Geophysical Data Center 1988). This page, left: Record mean (604 days) vectors. This page, right: Mean vectors for two 100-day periods of strong AABW transport (3 Oct 1992–11 Jan 1993 and 17 Sep 1993–26 Dec 1993). Next page, right: Mean vectors for two 50 day periods of weak AABW transport (12 Feb 1993–3 Apr 1993 and 12 Feb 1994–3 Apr 1994). Next page, left: Mean vectors for two 100-day periods of strong LNAADW transport: (7 Mar 1993–15 Jun 1993 and 18 Feb 1994–29 May 1994).

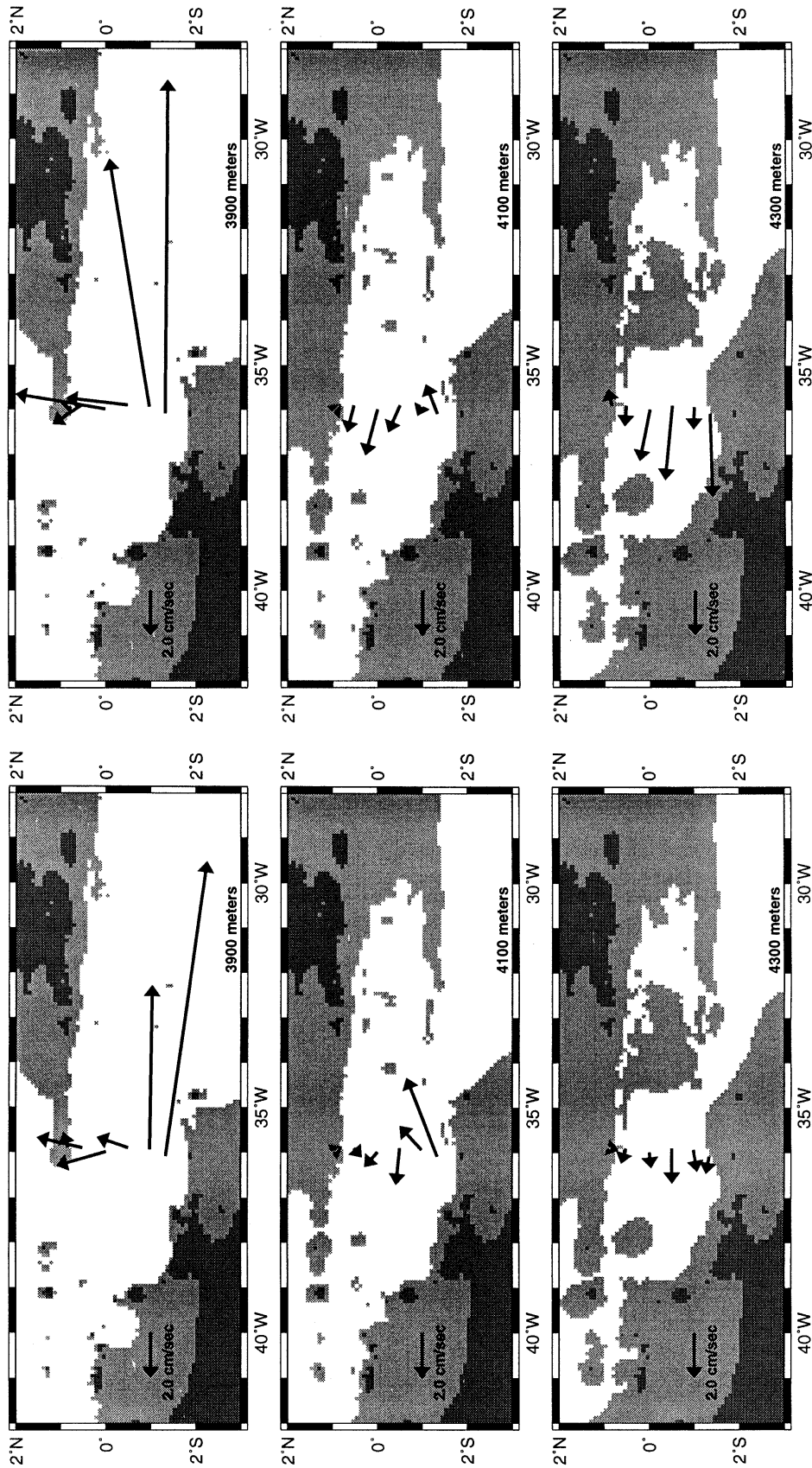


FIG. 4. (Continued)

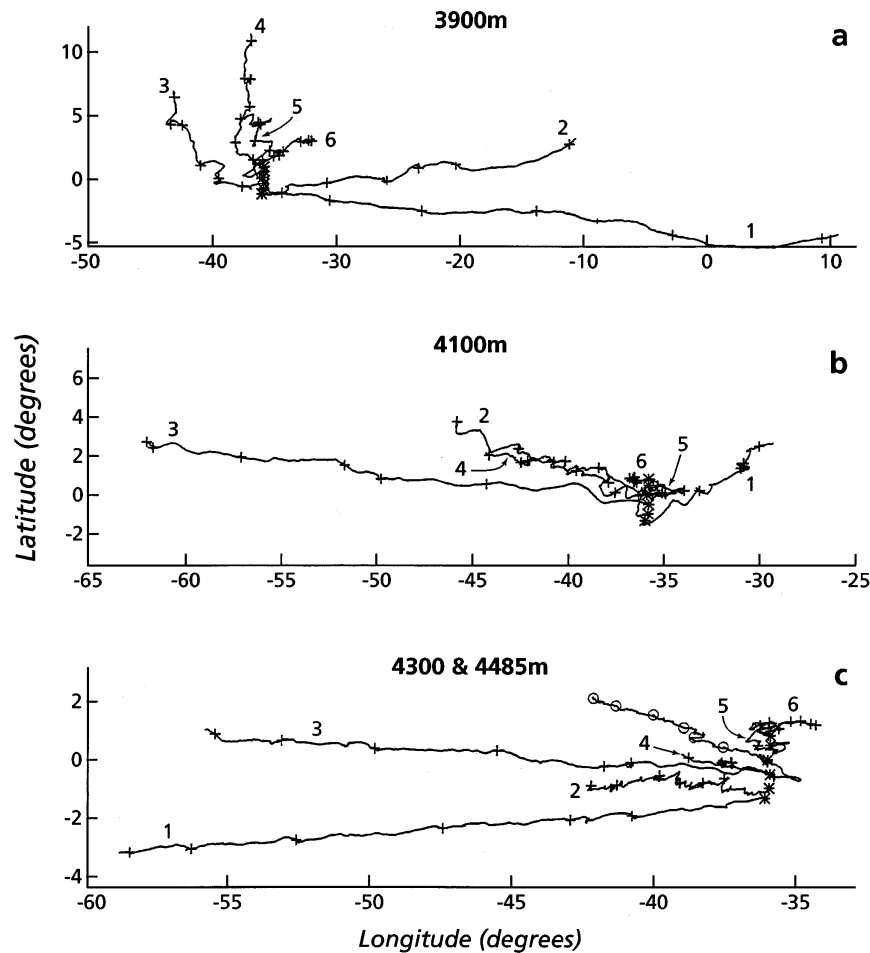


FIG. 5. Progressive vector diagrams for currents at (a) 3900 m; (b) 4100 m; (c) 4300 m and 4485 m (circles), from mooring 4. Asterisks mark the mooring locations; crosses are placed at 100-day increments.

for this water mass. One could simply use a depth such as 4000 m, which is roughly in the transition layer between AABW and NADW, but most investigators have used a potential isotherm to identify the top of the bottom water. For this transport calculation, the potential isotherm $\theta = 1.8^\circ\text{C}$ has been used to define the top of the AABW layer. This isotherm is near the top of the strong vertical temperature gradient where water properties change from NADW properties to AABW properties. This choice is also consistent with recent choices by others (Molinari et al. 1992; Friedrichs and Hall 1993), although it does differ from the choice of 1.9°C by Whitehead and Worthington (1982). Hence, alternative definitions are also presented. It will be shown that transport is not overly sensitive to the definition used. Without a continuous representation of either the flow field or the temperature field, the use of the 1.8°C isotherms involves, in essence, a double interpolation amongst the moored instruments. Details of the transport calculation are presented in appendix B.

Table 4 lists mean transports and standard deviations

for four definitions of AABW: $\theta = 1.8^\circ\text{C}$; $z = 4000$ m; $\theta = 1.7^\circ\text{C}$; and $\theta = 1.9^\circ\text{C}$. Those cases labeled A utilize the full array dataset. Cases labeled B use only the four southernmost moorings, as they have the preponderance of flow in the array. Summing all transport below 1.8°C through the channel yields an estimate for mean AABW transport of -2.0 Sv (Table 4, 1A). This is the sum of an organized westward flow of 2.24 Sv and a recirculating (eastward) flow of 0.24 Sv, which occurs at the 4100-m level at the southernmost mooring. Case 2 recognizes that the interpolation for 1.8°C is a bit more sophisticated than that possible for velocity and uses the alternative simpler AABW definition as water below 4000 m. This results in a mean westward transport of 2.18 Sv, the sum of organized westward flow of 2.31 Sv, and a weaker eastward recirculation of 0.13 Sv. Mean transport below $\theta = 1.7^\circ\text{C}$ is -2.06 Sv (westward flow of 2.18 Sv and eastward flow of 0.12 Sv); for $\theta = 1.9^\circ\text{C}$, the westward flow is similar (2.22 Sv), but the recirculation is much stronger (0.39 Sv), so the net is only 1.83 Sv westward. The 1.8°C isotherm lies above

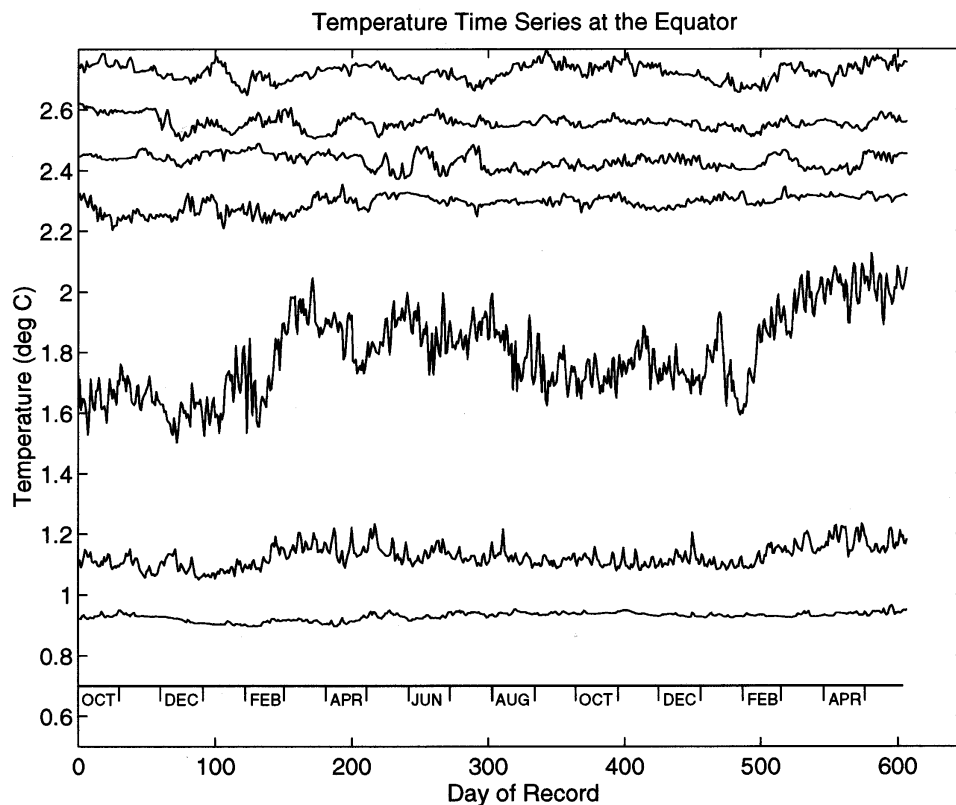


FIG. 6. Time series of in situ temperature at seven levels from the equatorial mooring. For depths of measurements see Table 3.

4000 m for most of the experiment at the southern two moorings (where the eastward flow of the southern boundary layer is found at 3900 m and intermittently at 4100 m). Thus, relatively more of this eastward flow is mapped onto the AABW layer for cases 1 and 4 ($\theta = 1.8^{\circ}\text{C}$, 1.9°C) than for cases 2 and 3 ($z = 4000$ m; $\theta = 1.7^{\circ}\text{C}$). Transports for the four cases are all within 10%–15% of each other because two-thirds of the transport occurs below 4200 m where $\theta < 1^{\circ}\text{C}$.

As noted in section 2, the strong eastward flows observed at the southern end of the array are associated with the flow of LNADW from the Guiana Basin to the Brazil Basin, the crossing of the equator by the deep western boundary current. This eastward flow includes water colder than 1.8°C from entrainment of AABW into the overlying jet. An estimated 1.24 Sv flows between 3800 and 4000 m, based on the record mean speeds at the southern two moorings, with corresponding temperature range of 1.8°C – 2.0°C . Rhein et al. (1995) use several Pegasus velocity sections along 35°W to estimate a transport of “old” NADW ($\sim 1.8^{\circ}\text{C}$ – 2.3°C) as 4.6 ± 2.6 Sv. Friedrichs et al. (1994) estimate about 7 Sv transequatorial LNADW transport between 1.8° and 2.4°C with 3 Sv of that colder than 2.0°C . Our array data represent only a small piece of this LNADW flow, which for the most part passes above the array, as well

as partly south of it, according to the Rhein et al. (1995) velocity and CFC-11 sections at 35°W .

Both the marginal spatial resolution of the array and the strong time variability of the records introduce a level of uncertainty in our transport estimates. To assess the effect of horizontal resolution, consider first the relatively low velocity measured at 4300 m near 1°S , mooring 2. Suppose that low speed is in error: using instead a zonal speed of -4.5 cm s^{-1} (the rough average of the -4.88 and -4.22 cm s^{-1} recorded at moorings 1 and 3, respectively) would increase the case 1 estimate in Table 4 by 15% from 2.0 to 2.3 Sv. One could go a step further and suppose that instead the 4300-m velocity distribution might be jetlike, with a maximum at this location. The three realizations of Pegasus sections by Rhein et al. (1995) and a fourth reported in Rhein et al. (1996) suggest such an AABW jet and show its westward speed maximum comparable to the eastward speed maximum of the overlying LNADW boundary layer eastward flow. The eastward LNADW maximum speed in the array is about 9.9 cm s^{-1} , and imagining an AABW jet with this speed westward at the problematic instrument would increase the case 1 transports by 40% from 2 to 2.8 Sv. While these uncertainty estimates focus on the problematic 4300-m instrument on mooring 2, they also provide some general indication of the ef-

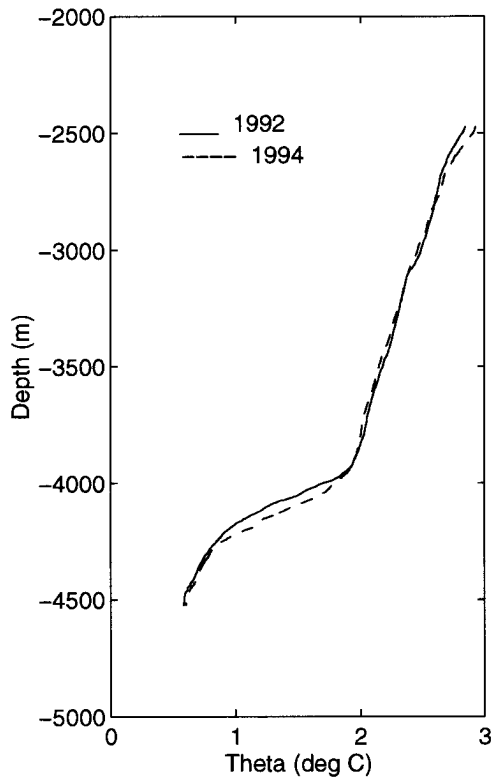


FIG. 7. Comparison of section-averaged vertical profiles $\theta(z)$ at deployment (solid) and at recovery (dashed).

fects of inadequate sampling resolution for flows of small horizontal scale. However, since smaller horizontal scales tend to be associated with higher frequencies, such errors should tend to average out over a long time. Thus, we expect that the most significant error due to horizontal resolution is that associated with the anomalous instrument record described above.

It is similarly difficult to estimate uncertainties of vertical resolution—harder than for an extra-equatorial array where geostrophy provides a natural shear estimate for comparison with the current meter shears. In our array, only mooring 1 in the south shows a simple mean vertical shear of the zonal currents: the others show varying shears and/or meridional components of flow between the three levels. It is thus possible that sampling at the three primary levels of our array is inadequate for characterizing the depth-integrated AABW zonal speed. In addition, the equatorial mooring provides our only measurement of flow below 4300 m (Fig. 2; Table 3). Its average westward velocity of 1.3 cm s^{-1} at 4485 m is actually stronger than the average at 4285 m (0.6 cm s^{-1} westward) on the same mooring. However, the 4300-m measurements of the primary array dominate the AABW transport estimate at the other moorings, where we have no deeper speed measurements. Thus, the array may have failed to sample the AABW flow nearer the bottom, and the AABW transport may be underestimated by not allowing for shear

TABLE 4. AABW transport ($10^6 \text{ m}^3 \text{ s}^{-1}$), calculated as described in text (westward transport is negative). Cases 1A, B integrate transport below the 1.8°C isotherm. Cases 2A, B integrate below nominally 4000 m (actually below midpoint of current meters at nominal 3900- and 4100-m depths). For both 1 and 2, A refers to through channel transport; B integrates only over the southern four moorings (i.e., south of $\sim 0^\circ 15' \text{N}$). Cases 3 and 4 integrate transport below the 1.7° and 1.9°C isotherms, respectively.

Case	Mean	Std dev	Max	Min	Top of AABW
1A	-1.99	1.58	2.33	-8.68	$\theta = 1.8^\circ\text{C}$
1B	-2.01	1.39	2.01	-7.26	$\theta = 1.8^\circ\text{C}$
2A	-2.18	1.61	2.30	-8.58	4000 m
2B	-2.19	1.42	1.82	-7.19	4000 m
3	-2.06	1.54	2.19	-8.34	$\theta = 1.7^\circ\text{C}$
4	-1.83	1.63	2.55	-8.94	$\theta = 1.9^\circ\text{C}$

between 4300 m and the sea floor. Fortunately, undetected near-bottom shear is not likely to greatly enhance the AABW transport since an extra 0.7 cm s^{-1} speed in the bottom 150 m across the entire width of the array would boost the transport by only 0.4 Sv. The presence of significant northward flow components at some depths should not introduce additional uncertainty: through channel transport depends only on the velocity component normal to the channel cross section, that is, zonal velocity.

The time series of daily average through channel transport of water colder than 1.8°C is shown in Fig. 8, along with the 40-day running mean; time series for all other cases except case 3 would be nearly indistinguishable from this. In an event near the start of the daily averages, maximum westward transport exceeds 8 Sv, and at times the flow reverses to eastward with total transport as high as 2 Sv. Although standard deviations for the different transport time series are 65%–80% of the record means, the integral timescale for transport is about 10 days, suggesting about 60 degrees of freedom for the 604-day-long record. Using $N = 60$ yields standard errors on the order of 10% of the means. In addition to the obvious high-frequency content of the time series, there is a seasonal cycle visible in the 40-day filtered curve: this results from the above-described periods of strong and weak AABW velocity vectors. The record is not long enough to constrain a seasonal cycle, nor to isolate it as a spectral peak, but the appearance of a quasi-annual cycle is striking none the less: the record begins with strong AABW transport and has a second strong period about a year into the record. In addition, there are weak AABW transport periods about one-half year into the record and again about one and a half years into the record. Notable peaks in the power spectrum for the transport time series occur at 120 days and at periods of 50–60 days, as well as in the band from 25 to 30 days. Whitehead and Worthington (1982, near 4°N) and Johns et al. (1993, 8°N) found a prominent 60-day periodicity in the bottom water velocities, but the 120-day period has not been observed before, as far as we know. The AABW transport minima in Fig. 8 are

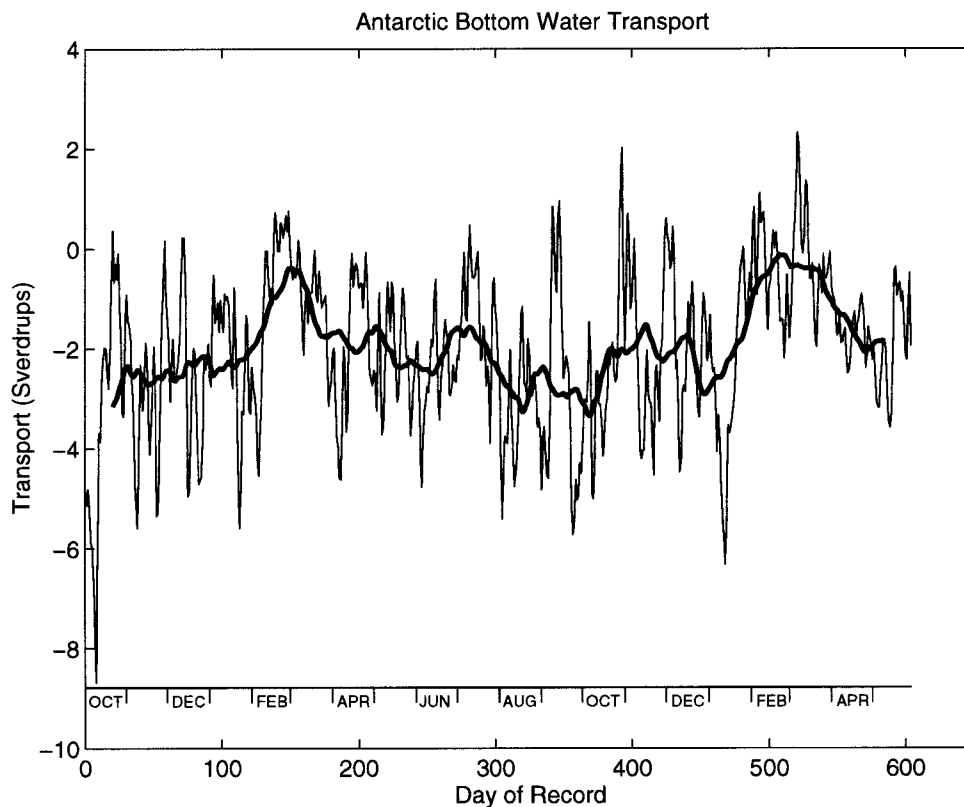


FIG. 8. For the 604-day experiment the daily average transport of AABW defined as water with $\theta < 1.8^\circ\text{C}$, estimated as described in the text from the daily average westward flow speeds and potential temperatures. Superimposed is the running 40-day (boxcar) filtered AABW transport.

rather sharply peaked in time due to the interaction of the 120-day and seasonal cycles. As noted in the discussion of Fig. 4, the LNADW also has a seasonal cycle with a strong eastward flow phase in the south that lags

the weak AABW phase by about a month. This delay is particularly visible in the time series of vector velocity, Figs. 3a-c.

To assess the effect of the lower-frequency variability on the calculations of mean transport, the time series was fitted with a model that included a seasonal harmonic and a 122-day cycle (one-third of a year). It was also necessary to include a term that could describe the long-term trend observed in the transport: in particular, the 365-day running mean persistently declined from 2.2 to 1.9 Sv westward (Fig. 9). Details of the fits are given in appendix C. In summary, using a linear term in the model leads to a mean transport of exactly 2 Sv if we extrapolate to a full two years. On the other hand, the transport is not expected to decrease indefinitely. Modeling the "trend" instead as part of a two-year-long cycle leads to a mean transport of 2.14 Sv westward over a full two years, an increase of about 7%.

Naturally it is impossible to determine variability of the current for times longer than or equal to the 604-day sampling period, but we can assess the stability of our transport estimate by computing the mean over subsets of the time series. Table 5 shows the mean transport over 604 days, and means over sequential intervals of 302, 151, and alternating 75 and 76 days. The 302-day values differ from the 604-day value by just 3%, but

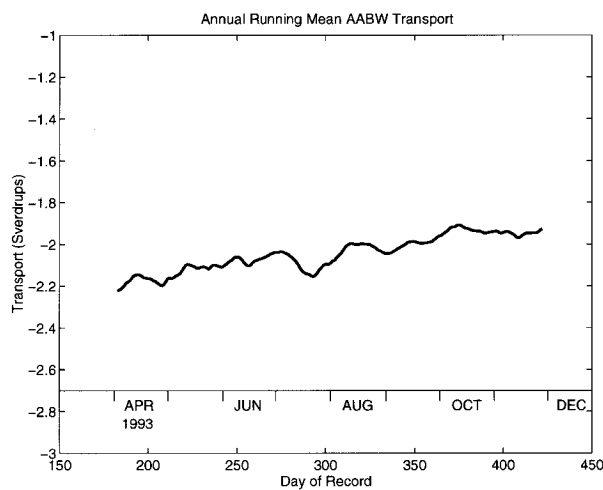


FIG. 9. The running yearly (365-day boxcar) averaged transport of AABW defined as the water with $\theta < 1.8^\circ\text{C}$. The filtered time series begins at day 183 of the daily average transport time series of Fig. 8, and the last day is day 422 of the daily series.

TABLE 5. AABW volume fluxes averaged over assorted time intervals, from top to bottom: 604 days; 302 days; 151 days; 75/76 days. Flux is westward and units are Sverdrups.

1.99							
2.06				1.93			
2.32		1.79		2.49		1.37	
2.77	1.88	1.50	1.99	3.04	1.94	1.21	1.52
151		302		453		604	
Day Average							

the similarity of these numbers is deceptive for it reflects that the array deployment coincided with the maximum transport phase. A running 302-day mean yields values ranging from -1.86 to -2.34 Sv, which differs from the 604-day value by up to 15%. Figure 10 shows the running 40-day mean volume flux from Fig. 8 as well as the values from Table 5. In addition to the seasonal cycle with annual minima in late February/early March, the intermediate minima near 280 days and 400 days are evidence of the 120-day signal noted above. This appears to reinforce the seasonal minima at 160 days and 520 days and may account for the sharpness of the annual minima, and the flatness of the annual maxima. The 151-day mean values (triangles in Fig. 10) begin to define the annual signal and the 75/76 day averages (\times 's in Fig. 10) show it even more clearly. The variation of these transport estimates over subsets of the data show that shorter current meter records could have been misleading.

4. Discussion

For the 604 days of the current meter array velocity data we estimate that between 2.0 and 2.2 Sv of AABW flowed through the array (Table 4), and thus from the Brazil Basin of the South Atlantic into the Guiana Basin of the North Atlantic. This measured AABW flow was southern intensified within the equatorial channel, and recorded almost completely by the four moorings that were placed between 1.3°S and the equator, with negligible flow recorded at two moorings north of the equator. Therefore, even though the array is in the extreme northwestern "corner" of the Brazil Basin, the crossing of the equator by the AABW is achieved west of the array. Given the restriction of the AABW to depths greater than 4000 m, the bathymetry of Fig. 1c shows this crossing must occur between the longitude of our array, 35.9°W , and 39° – 40°W , a zonal width of 350 to 450 km, about twice the meridional width of the westward flow through our array. The space available, and the shape of the bathymetry, are such that this crossing can occur at about a 30° angle from westward without requiring a narrowing of the current as it crosses. At the colder sampled level of 4300 m, Fig. 4, the distance to the western boundary from the array is only about

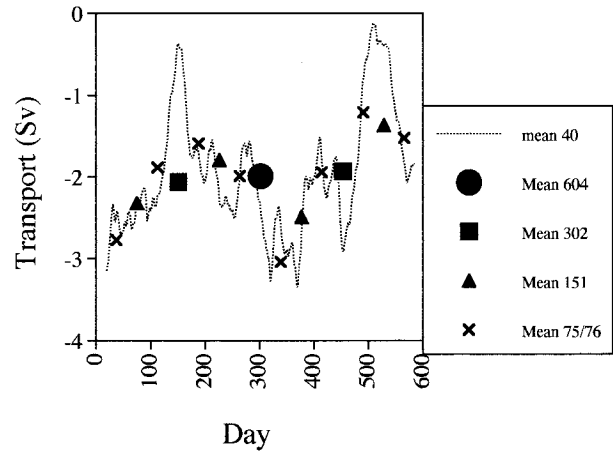


FIG. 10. The 40-day filtered AABW transport estimate for AABW defined as water with $\theta < 1.8^{\circ}\text{C}$, from Fig. 8, compared with several bulk averages: the record mean, and means for successive record halves, quarters, and eighths.

320 km, requiring a larger turning angle for the cold AABW unless it rises as it turns across the equator. The mean velocity vectors at this level of the array show only about a 5° veering of the flow to the north of westward, Fig. 4a, and thus the veering of the 4300-m flow from westward to flow northward across the equator must be quite abrupt as it has barely begun at our array.

Did we measure the total AABW flow that passes from the Brazil Basin to the Guiana Basin with our array? There are two sorts of uncertainties. The first set comprises issues of the horizontal and vertical sampling, as discussed already. The second is the possibility of other pathways for cross-equatorial flow outside the domain sampled by the array. The latter issue depends on the accuracy of a variety of bathymetric datasets, including the contoured one in Fig. 4, which portray the Parnaiba Ridge as a continuous southern wall to the equatorial channel westward of our array; these data were also used as a guide in selecting a longitude sufficiently far east that the north channel wall is a continuous barrier to northward AABW flow east of our array. Overall, bathymetric data densities are much greater for the Parnaiba Ridge than for the north wall, and thus the possibility of a leak somewhere east of the array is of greater concern than for leaks through the Parnaiba Ridge west of the array. We know of no particular evidence of such a leak, but simply do not have enough bathymetric data to rule out the possibility altogether.

The three temperature sections (Fig. 2) present a bit of a paradox, for they show the coldest AABW, $\theta \leq 0.6^{\circ}\text{C}$, north of 0.4°S , in spite of the bulk of the estimated transport of AABW being south of there. North of the equator the 4300-m instruments indicated negligible flow. Perhaps the coldest water there migrated northward beneath the relatively motionless 4300-m

TABLE 6. Estimates of AABW transport in the South Atlantic (Brazil Basin), North Atlantic (Guiana Basin), and near the equator. "RL" means reference level (level of no motion).

Reference	Location	Transport (Sv)	Comments
<i>Brazil Basin</i>			
Wright (1970)	8°S	2.8	RL = top of LNADW to AABW transition
McCartney and Curry (1993)	11°S	5.5	RL = 1.9°C; water below 1.9°C
Speer and Zenk (1993)	11°S	3.0	RL = 2.1°C; same data as McCartney and Curry; different bottom triangle treatment
DeMadron and Weatherly (1994)	15°S	4.4	RL = 1.9–2.0°C ($\sigma_4 = 45.87 \text{ kg m}^{-3}$)
<i>Guiana Basin</i>			
Wright (1970)	8°N	2.7	RL = top of LNADW to AABW transition; inappropriate RL for GB.
Whitehead and Worthington (1982; "WW82")	4°N	1	Current meters; flow over Ceara Rise only
WW82	4°N	2 (2.3)	RL = 1.9°C; total flow, Ceara Rise to Mid-Atlantic Ridge; computational error raises estimate to 2.3 (Luyten et al. 1993).
McCartney and Curry (1993)	4°N	4.0	Used WW82 data; RL = 1.9°C; different bottom triangle treatment
Luyten et al. (1993)	4°N	3.2–4.0	Water below $\theta = 1.9^\circ\text{C}$; varying RL
McCartney et al. (1991)	11°N	2.2	Water colder than 2°C; flow is through Vema Fracture Zone into eastern basin
Friedrichs and Hall (1993)	11°N	2	Net for entire transect; negligible net flow in Guiana Basin
<i>Equator</i>			
McCartney and Curry (1993)	37°W	4.3	RL = 4000 dbar ($\theta \approx 1.93^\circ\text{C}$); equatorial geostrophy
Rhein et al. (1995)	35°W	0.6, 2.6, 4.6	Pegasus sections
Rhein et al. (1996)	35°W	1.8	Pegasus section

level north of the equator. Such flow is hinted at by the mean current measured at the deepest instrument on the equatorial mooring, which is oriented 20° north of west. Again, however, these considerations presumably involve relatively small transports of a few tenths of a Sverdrup.

How does our AABW transport compare with previous estimates of Atlantic AABW circulation? The earliest attempt to estimate AABW transport through the western basin used the *Meteor* data from the 1920s (Wüst 1957) but was not successful due to coarse resolution. Since then many estimates have been made in both the Guiana Basin of the North Atlantic and the Brazil Basin of the South Atlantic. Some of these appear in Table 6. Note that AABW transport from the Brazil Basin supplies not only the northward flow into the Guiana Basin that we attempted to measure, but also the eastward flow through the Romanche and Chain Fracture Zone into the eastern basin. From Table 6, roughly 3 to 5 Sv of AABW is approaching the equator from midlatitudes of the Brazil Basin (no estimates of the effect of time variability were made). The amount is smaller than the 7 Sv estimated entering the Brazil Basin from the south (Speer and Zenk 1993) presumably because of upwelling within the basin. Our array estimate of somewhat more than 2 Sv continuing into the Guiana Basin implies that between 1 and 3 Sv is available for the combination of the eastward flow through the Romanche Fracture Zone and the upwelling from AABW into the LNADW in the Brazil Basin.

In the Guiana Basin, there is a strong recirculating gyre in the deep-water and AABW circulation (Friedrichs and Hall 1993), and a deep level of no motion is inappropriate. At a minimum, a level of no motion is required above the deep water. Thus, Wright's calculations in the Guiana Basin, though fortuitously close to ours, are flawed; indeed, they simultaneously give a net deep-water flow that is northward rather than southward. Four estimates are presented for flow of AABW near 4°N, all based on the current meter and/or hydrographic data presented in Whitehead and Worthington (1982). These all use a reference level of 1.9°C, but the estimates range from 2 to 4 Sv for the total flow between the Ceara Rise and the Mid-Atlantic Ridge. The very rough topography at the 4°N section makes the estimates of near-bottom shear and transport speculative since there is no clear evidence that the gaps connect to the north. Moreover, the time variability of the current is known to be significant, and no single geostrophic calculation can estimate the mean flow.

Another recalculation of this 4°N transport is given in Luyten et al. (1993) showing the dependence of the transport colder than 1.9°C on an assumed level of no motion that ignores the current meter measurements supporting 1.9°C. In such a case, there is a gyre aspect to the shear and flow east of the Ceara Rise, and raising the level of no motion primarily increases the gyre intensity while the net northward transport of AABW stays in the range 3.2–4.0 Sv. In particular, using a reference level of 3.2°C, deduced as optimal by Fried-

richs and Hall (1993) for a location farther north, Luyten et al. (1993) show a transport of 3.6 Sv. This is larger than our transequatorial estimate, which could reflect the inclusion of some northward recirculating LNADW in the 4°N estimate, through the use of 1.9°C as the top of the AABW, and the exclusion of the southward flowing waters between 1.7° and 1.9°C over and west of the Ceara Rise. In addition, there could be entrainment of LNADW into the AABW as the mechanism of progressively warming the AABW as it flows northward. Thus, although the use of 1.9° as a reference level as tested by current meters by Whitehead and Worthington (1982) may be correct, the northward modification of AABW through mixing complicates comparisons of transport.

Farther north in the Guiana Basin, McCartney et al. (1991) estimated a flow of about 2.2 Sv colder than 2°C debouching from the Vema Fracture Zone into the eastern North Atlantic. The immediate source of that water is the northward flow of AABW in the Guiana Basin, part of which is diverted to the eastern basin by the flow through the Vema. At the point where this transport estimate applies, well eastward along the Vema, the coldest water is 1.58°C, considerably warmer than the water entering the Vema from the northward flowing AABW in the Guiana basin, where bottom temperatures are about 1.27°C. How much the entrainment of overlying deep water has increased the transport in the process of raising the temperature as the water passes through the Vema is of course unknown, so it is not possible to estimate what fraction of the AABW (and entrained LNADW) flowing northward near 10°N in the Guiana Basin is diverted eastward into the Vema, other than an expectation that it is less than 2 Sv.

Friedrichs and Hall (1993) examined a full North Atlantic transect that falls near 11°N. The use of a full ocean section has the advantage of allowing rigorous application of overall mass balance. The section is completely north of the Vema Fracture Zone through the Mid-Atlantic Ridge. East of the ridge they found a net northward transport of AABW amounting to 2 Sv, but negligible net northward transport of AABW west of the ridge. This most likely reflects inadequate sampling along the western flank of the Mid-Atlantic Ridge, where the colder classes (and strong flow) are not resolved due to a large bottom triangle at the critical station pair where the northward flow is concentrated. With the northward flow underestimated because of this difficulty, the recirculating southward flow of AABW in the deep western boundary current essentially cancels the northward flow.

Some estimates of AABW transport right at the equator also exist (Table 6). McCartney and Curry's rather high estimate of 4.3 Sv falls within the rms of the daily transport estimates, but is outside the range of the 40-day filtered transport estimates (Fig. 8). But the 1983 section (Fig. 1c) was in the area where there must be a significant northward flow (see above). Rhein et al.

(1995) estimated AABW transports just east of our moored array site using three Pegasus sections (Table 6). Their reported AABW transport of $2.6 \text{ Sv} \pm 2 \text{ Sv}$ is the average and standard deviation of these three estimates, one of which they describe as "not well resolved" due to station spacing. The third section was made about 50 days into our moored experiment, when the 40-day filtered time series shows 2.4–2.6 Sv of AABW flow, agreeing well with the 2.6 Sv they measured. On the other hand, the daily average transport time series, Fig. 8, shows much larger fluctuations, from greater than 5 Sv westward to essentially zero westward transport. Indeed, the plot of daily average array transport is not particularly encouraging for the use of a small number of velocity snapshots to define the mean flow. A fourth Pegasus section (Rhein et al. 1996) was made from a cruise in February–March 1994, about 75 days before the end of our moored experiment. Its estimated westward transport lies in the range of daily transports (2 Sv westward to 2 Sv eastward), while the 40-day filtered transports, Fig. 8, show this period as the second transport minimum of the record.

As mentioned in section 2d, the moored array data and the supporting hydrography both indicate a warming trend over the duration of the experiment. The cold AABW at 4300 m warmed at a rate of 0.016°C/yr; this can be compared to a rate of warming found by Zenk and Hogg (1996) for the coldest AABW entering the Brazil Basin through the Vema Channel of 0.015°C/yr over a two year stretch (1991–92). They noted that sporadic data at this site back through 1973 indicates that coldest temperatures were stationary in the range -0.17° to -0.19°C , with the warming from that range to -0.13°C during the experiment therefore looking highly anomalous. Coles et al. (1996) have documented a shift in the distribution of coldest levels of AABW in the Argentine Basin in the late 1980s, whose subsequent advection (with mixing) into the Vema Channel might be related to this warming signal. At our site on the equator, the overall history is somewhat different. Data within 10–100 km of the array in the equatorial channel in 1972, 1983, and 1989 all show coldest AABW temperatures quite close to each other (0.611° , 0.617° , and 0.612°C), and all warmer than our observations (0.582° – 0.595°C) by about 0.03°C. Thus, the warming trend during the experiment may be a recovery phase from some cooler period between the earlier warmer period and the experiment. At the Vema Channel the warming period described by Zenk and Hogg (1996) may be a response to an earlier warming event of the upstream source for the Vema waters. At the equator we can speculate on a somewhat different scenario.

As the AABW flows from the Brazil Basin to the Guiana Basin it warms considerably. Basically this reflects vertical exchange between the AABW flowing one direction beneath the LNADW flowing in the other direction (although by no means do the cores of current lie over each other). The near-bottom temperature has

a large gradient northward from the site of our experiment into the Guiana basin. For example, Whitehead and Worthington found the coldest AABW at 4°N in 1977–78 to be 0.99°C, and based on the historical data just described, at that time the coldest AABW at our array location was 0.61°–0.62°C. The likely connecting pathway between the two locations is about 780 km, so the bottom temperature gradient is about .05°C/100 km. Thus, the 604-day warming trend can be interpreted as a shift of between 20 and 30 km of the bottom isotherms toward the Brazil Basin during the experiment. The other change during the experiment is the descent by order 25–40 m (after removing the seasonal effect) of the transition layer between the LNADW and the AABW, giving a distinct warming trend at the 4100-m level of our array and a weaker warming trend at the 4300-m level. There is little indication of change at the 3900-m level. The temperature sections, Figs. 2 and 7, confirm the warming trend at depth, but also show the trend passing from warming through zero to a slight cooling trend above 3900 m that fades away near 3000 m. Thus, by the end of the experiment, the LNADW has thickened, the transition layer has moved downward, accommodating the thickened LNADW, and the AABW layer has thinned with the coldest AABW getting warmer; the latter warming may be interpreted, as just mentioned, as a shift toward the Brazil Basin of the bottom temperature gradient that delineates the erosion and warming of the AABW as it flows into the Guiana Basin.

The counterflow arrangement of the LNADW and AABW, and the quasi-stationary mixing between them, are the fundamental basis for interpreting the distribution and variation of these water masses. In particular, the LNADW in the deep western boundary current in the southern Guiana Basin has a much thicker character, with its low vertical stratification extending to colder than 1.75°C, while in Fig. 2 the higher gradients of the transition layer reach warmer than 1.85°C, and at 11°S in the Brazil Basin the higher gradients reach warmer than 2.0°C (see, e.g., McCartney 1993). This progression, as well as the opposing progression of warming of the AABW layer toward the north, reflects the advective diffusive balance between these opposing flows. We thus are led to interpret the above summarized trends of thickening LNADW, thinning AABW, deepening of the transition layer, and warming of the coldest AABW as indicative of a shift in this balance toward a stronger LNADW influence and a weaker AABW influence. A natural candidate for such a shift is that the period of our experiment corresponds to one where the LNADW transport is stronger than the preceding period and/or the AABW transport is weaker; a geographical shift of the thermal structure gives all of those trends. Indeed, as discussed in section 3 and appendix C, there is evidence that AABW transport weakens over the 604-day observation period. However, while the fits are useful for eliminating the seasonal signal to estimate mean AABW transport, the transport record is too short to

unambiguously resolve and quantify the overall trend. It is interesting that Zenk and Hogg (1996) found that the two-year warming of the coldest AABW in the Vema Channel in 1991–92 was accompanied by decreased geostrophic shear and a decline in net AABW transport between the Rio Grande Rise and South America from about 6 to 4–5 Sv.

The 4100-m temperature records across the array, Fig. 3e, lend credence to the idea that the movement up and down of the transition layer does, in general, track on the waxing and waning of AABW transport. Recalling that the AABW transport, Fig. 8, is greatest in September–October and smallest in February–March, followed by greatest LNADW transport in April–May, we see that superimposed on the overall warming trend at 4100 m are relatively cold events (uplifted transition layer) during the strong AABW periods (a shift of the LNADW/AABW balance toward the Guiana Basin reflecting stronger AABW influence all across our array) and relatively warm events (depressed transition layer) during the weak AABW and strong LNADW periods (a shift of the LNADW/AABW balance toward the Brazil basin reflecting enhanced LNADW and diminished AABW influence all across the array). Since the seasonality of AABW transport is tracked by the vertical excursion of the transition layer, it seems plausible that the overall descent of the transition layer during our 604-day experiment may indicate declining AABW transport.

5. Summary

As part of the Deep Basin Experiment of the international efforts of the World Ocean Circulation Experiment, an array of six moorings was deployed for 604 days at abyssal levels in the western Atlantic Ocean. The goal was to measure the net flow of AABW from the Brazil Basin of the western South Atlantic into the Guiana basin of the western North Atlantic. This overall northward flow locally becomes westward along the equator because of an abyssal channel: northward flow of AABW enters the eastern end of the channel eastward of 32°W, is constrained to flow westward along the equator to 38°W, and debouches northward onto the Ceara Abyssal Plain of the Guiana Basin westward of 38°W. The moored array at 36°W spanned this channel and thus sampled the total AABW flow.

Several estimates are made of the average AABW transport for the 604-day record. The first uses an estimate of the depth of the $\theta = 1.8^\circ\text{C}$ isotherm at each mooring and yields 2.0 Sv below that temperature. The second uses 4000 m as the bounding surface for the AABW and yields 2.2 Sv below that surface. Transport is also estimated for bounding isotherms of $\theta = 1.7^\circ\text{C}$ and $\theta = 1.9^\circ\text{C}$. In all four transport estimates, organized westward flow of 2.2–2.3 Sv is partially compensated by eastward recirculation of 0.1–0.4 Sv, which occurs at 4100 m at the southern end of the array. Above this,

the strongest average speed of the whole array was recorded: an eastward flow of nearly 10 cm s^{-1} , representing the northern edge of a southern boundary current that conveys LNADW into this northwestern corner of the Brazil Basin.

The directions of the significant currents sampled by the array are persistent, but there is considerable low-frequency variability of the individual speeds at frequencies from daily through seasonal, and these fluctuations carry over into the AABW transport estimates. Using the integral timescale of 10 days, we estimate standard errors of about 10% for the means. Sparse sampling in the horizontal and vertical most likely leads to underestimating the transport. The largest such error is probably that associated with the 4300-m instrument on mooring 2 at 1°S , where flow was relatively weak as the mooring was in the wake of a topographic feature. This error is estimated to be 0.3–0.8 Sv (15%–40%) depending on the details of the flow structure. An annual cycle is tantalizing, though indeterminate given the 604-day duration of the experiment. The AABW transport, low-pass filtered at 40 days to suppress higher-frequency fluctuations, begins the record (September–October 1992) with strong westward transport greater than 3 Sv, but declines to a minimum of only about 0.3 Sv by February–March 1993. The transport then recovers to the same high value above 3 Sv in September–October 1993, then repeats the decline to a minimum of 0.1 Sv in February–March 1994. The recovery toward high transports after this second minimum is cut short by the array recovery since the record is shorter than two years. If the transports are indeed annual, then extrapolation for the additional 126 days to complete a full two cycles would elevate the above transport estimates by order 7%. The simplest description of the interhemispheric AABW flow is that it is southern intensified within the equatorial channel at an amplitude of 2.0–2.2 Sv, with an annual cycle about that mean that waxes to a maximum transport of 3.1 Sv in September–October and wanes to a nearly vanishing transport of 0.2 Sv in February–March.

The field of abyssal temperatures across the channel, as sampled by the moored instruments and by hydrographic section measurements near the times of array deployment and recovery, show a progressive warming corresponding to a descent of the isotherms that define the transition between the AABW and the overlying LNADW amounting to 50–80 m. About half is due to the seasonal cycle and half to a longer term trend. At 4100 and 4300 m the warming rates were 0.098°C/yr and 0.016°C/yr . The coldest observed AABW temperatures in the hydrographic measurements warmed from 0.582°C at deployment to 0.595°C at recovery, but it is impossible to say how much of this warming is due to a trend and how much to the seasonal cycle. In fact, the 604-day warming may actually be a recovery from some cooler phase before the experiment, as measurements within 10–100 km of this longitude in the channel in

1972, 1983, and 1989 were warmer by 0.02 – 0.03°C . In general, during the experiment the quasi-annual waxing and waning of AABW transport is reflected by the AABW transition layer rising and falling, the AABW thickening and thinning, and the LNADW thinning and thickening. We thus speculate that the overall trend in the experiment of a deepening transition layer means that the experiment overall is in a period of waning AABW transport.

Acknowledgments. We are extremely grateful to Dick Limeburner who was responsible for acquisition of the CTD data, Scott Worrirow who conducted the current meter operations, and Susan Tarbell who analyzed the current meter data. In all these cases the results are exceptionally good and it has been a pleasure to work with them. We also thank our Brazilian colleagues Anna Maria Scofano and Friedrich W. Herms and his students for assistance at sea. We received fine cooperation from Master Michael Dick of R/V *Iselin* and his crew and Master Carl Swanson of R/V *Knorr* and his crew, and we thank them all. Comments from referees greatly improved the final version of this paper. Thanks to Deborah Taylor for typing the manuscript. This research was supported by the Division of Ocean Sciences, National Science Foundation under Grant OCE91-05834.

APPENDIX A

Calculating θ from T Time Series

First we calculate section-averaged profiles of θ and S for both 1992 and 1994, which we denote $\bar{\theta}_{92}$, \bar{S}_{92} , $\bar{\theta}_{94}$, \bar{S}_{94} . For each $T(t)$ measurement we use the Fofonoff and Millard (1983) formulas to compute $\theta(t) = \theta(T(t), P_0, S_0)$, where P_0 is the (fixed) pressure at the mooring depth and S_0 is a time-weighted average of the salinity values from the CTD data at pressure P_0 . Using this value of θ , we then “look up” more exact salinity values from each of the two tables of $\bar{\theta}_n$, \bar{S}_n ($n = 1992, 1994$), which we will denote S_1 and S_2 . Next, two new values of θ are evaluated from $\theta_i(t) = \theta(T(t), P_0, S_i)$, $i = 1, 2$ (corresponding to 1992 and 1994). The process is repeated until it converges, which is usually after the first iteration. Finally, we linearly interpolate in time between the two θ values corresponding to 1992 and 1994, to obtain the final value $\theta(t)$ for that time and location.

APPENDIX B

Transport Calculation from T, u Time Series

The first step in the calculation was to estimate the depth z_0 of the 1.8° isotherm at each of the mooring locations. As noted at the end of the last section, potential temperature time series have been calculated for all moorings, so these were used in conjunction with the known instrument depths to create a time series of z_0 for each location. Although $\theta = 1.8^\circ\text{C}$ nearly always

fell between the instruments at 4100 and 3900 m, it is inappropriate to obtain z_0 by linear interpolation between their daily measured temperatures. Because θ_{3900} usually lay above the strong gradient region, linear interpolation would predict a z_0 that is too shallow.

Recognizing the inappropriateness of a linear temperature interpolation we instead used the linear fits for $\theta(z)$ calculated from the CTD data (see section 2e) as follows: Note that the calculated slopes are a good representation of the strong gradient region over the range $\theta \approx 1.0^\circ\text{--}1.85^\circ\text{C}$ in both 1992 and 1994. At 4100 m potential temperature θ always lay within this range, while at 3900 m temperatures $\theta < 1.85^\circ\text{C}$ occurred only twice at mooring 6, four times at mooring 2, and less than 5% of the time at mooring 1 (mostly at the beginning). Thus, we allowed for two cases when evaluating z_0 . 1) When $\theta_{3900} > 1.85^\circ\text{C}$, which was most of the time, we extrapolated upward from the 4100-m measurement to obtain z_0 (1.8°C):

$$z_0 = z_{4100} + \text{slope} \times (1.8 - \theta_{4100}),$$

where ‘‘slope’’ is the time-interpolated value of $dz/d\theta$ using the average 1992 and 1994 slopes at that θ from the CTD data. Here z_{3900} and z_{4100} are the actual rather than nominal depths of the current meters. 2) In the few cases when $\theta_{3900} \leq 1.85^\circ\text{C}$, both temperatures were in the strong linear gradient region, and it was more sensible to interpolate between them:

$$z_0 = z_{4100} + \frac{1.8 - \theta_{4100}}{\theta_{3900} - \theta_{4100}}(z_{3900} - z_{4100}).$$

Applying this method to all six locations, we obtained time series $z_0(t; 1.8^\circ\text{C})$ at each one. Jumps in z_0 from case 1 to 2 occurred almost exclusively at mooring 1. Though they caused high-frequency transport changes as large as 1 Sv, the effect on the mean and low-frequency total transport was negligible.

It was then relatively straightforward to integrate in y and z to obtain transport time series. Integration was trapezoidal in both the horizontal and vertical. Thus, areas associated with the velocities at each of the six instruments extend halfway to the next instrument (or the channel edges) horizontally, and halfway to the next instrument (or all the way to the bottom) vertically, except at 3900 m where the upward extension was taken to be 100 m. (Since all the AABW lies below 3900 m, this choice has no effect whatsoever on the bottom water transports.) Eastward velocities are multiplied by these areas to obtain transports associated with each instrument, and then percentages of the transports at 3900 or 4100 m lying above and below the 1.8°C isotherm were calculated using $z_0(t)$ from above.

APPENDIX C

Trend Fitting of the Transport Time Series

Visual inspection of the 40-day low-passed time series of transport suggests fitting it with both a seasonal

TABLE C1. Parameter values for least squares fits to transport time series. Phase shifts are relative to a start date of 3 Oct 1992.

	Functional			
	a	b	Fit	
			c	d
	η	ϕ	ψ	
C.1	-2.54	1.47×10^{-3}	-0.826 0.294	0.666 4.46
C.2, $n = 2$	-2.14	0.338 2.69	-0.969 0.271	0.642 4.45
C.2, $n = 3$	-2.28	0.449 3.75	-0.907 0.311	0.655 4.46
C.2, $n = 4$	-2.48	0.638 4.33	-0.889 0.325	0.659 4.47

component and one that has a 122-day period. (Attempts to include a 60-day period as well were unsatisfactory.) The longer-term trend revealed by the annual running mean transport (Fig. 10) is accommodated by either a linear trend, or a periodic component of low frequency. The fits are of the form

$$a + bt + c \cos(\omega t + \phi) + d \cos(3\omega t + \psi) \quad (C1)$$

or

$$a + b \cos\left(\frac{\omega}{n} + \eta\right) + c \cos(\omega t + \phi) + d \cos(3\omega t + \psi), \quad (C2)$$

where $\omega = 2\pi/1$ yr and $n = 2, 3, 4$. Variables a, b, c, d, ϕ, ψ , and η are free parameters. Least squares fits to the daily time series give the results in Table C1. The four fits and the 40-day running mean are shown in Fig. C1: for the first 604 days, the fits are nearly indistinguishable. They then diverge rapidly with increasing

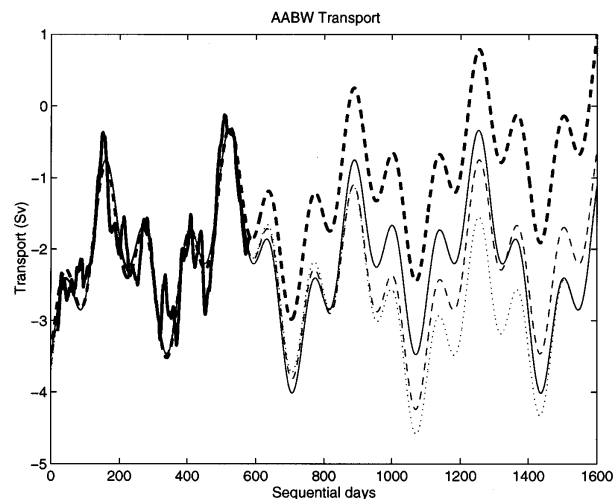


FIG. C1. Forty-day low-passed AABW transport (heavy solid curve), and four fits discussed in text: C.1 (heavy dashed curve); C.2, $n = 2$ (light solid curve); C.2, $n = 3$ (light dashed curve); and C.2, $n = 4$ (dotted curve).

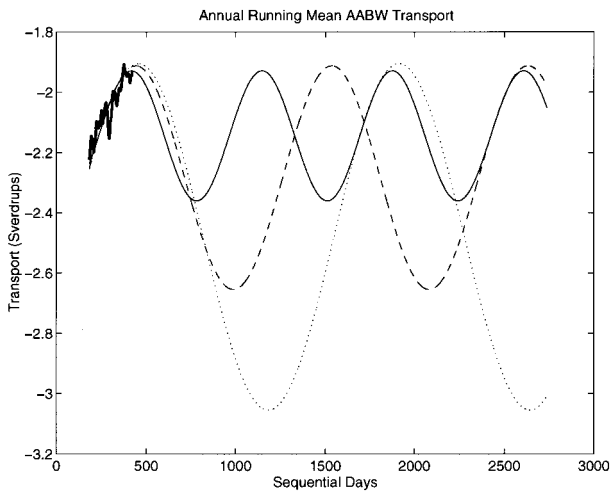


FIG. C2. Annual running means calculated for the periodic fits in C.2: $n = 2$ (solid), $n = 3$ (dashed), $n = 4$ (dotted), and the data (heavy solid curve).

time. As ω/n decreases, the total range of the functional fit (C2) increases, leading to ever larger (westward) long-term means for the transport (term “a” in Table C1). Figure C2 illustrates this effect by showing annual running means for the periodic fits: they track the running mean transport from the data initially, then diverge over their longer timescales. The “goodness of fit,” as measured by the rms difference between the measured and fitted transports, is the same within 1.5% for all four fits.

REFERENCES

- Coles, V. J., M. S. McCartney, D. B. Olson and W. M. Smethie Jr., 1996: Changes in Antarctic Bottom Water properties in the western South Atlantic in the late 1980's. *J. Geophys. Res.*, **101**(C4), 8957–8970.
- DeMadron, X. D., and G. Weatherly, 1994: Circulation, transport and bottom boundary layers of the deep currents in the Brazil Basin. *J. Mar. Res.*, **52**, 583–638.
- Fischer, J., and F. Schott, 1997: Seasonal transport variability of the deep western boundary current in the equatorial Atlantic. *J. Geophys. Res.*, in press.
- Fofonoff, N. P., and R. C. Millard Jr., 1983: Algorithms for computation of fundamental properties of seawater. UNESCO Tech. Papers in Marine Science No. 44, 53 pp. [Available from Division of Marine Sciences, UNESCO, Place de Fontenoy, 75700 Paris, France.]
- Friedrichs, M. A. M., and M. M. Hall, 1993: Deep circulation in the tropical North Atlantic. *J. Mar. Res.*, **51**(4), 697–736.
- , M. S. McCartney, and M. M. Hall, 1994: Hemispheric asymmetry of deep water transport modes in the Atlantic. *J. Geophys. Res.*, **99**(C12), 25 165–25 179.
- Hogg, N. G., P. Biscaye, W. Gardner, and W. J. Schmitz Jr., 1982: On the transport and modification of Antarctic Bottom Water in the Vema Channel. *J. Mar. Res.* **40**(Suppl.), 231–263.
- , W. B. Owens, G. Siedler, and W. Zenk, 1996: Circulation in the Deep Brazil Basin. *The South Atlantic: Present and Past Circulation*, G. Wefer, W. H. Berger, G. Siedler, and D. Webb, Eds., Springer-Verlag, 249–260.
- Johns, W. E., D. M. Fratantoni, and R. J. Zantopp, 1993: Deep western boundary current variability off northeastern Brazil. *Deep-Sea Res.*, **40**, 235–255.
- Luyten, J., M. S. McCartney, H. Stommel, R. Dickson, and E. Gmitrowicz, 1993: On the sources of North Atlantic Deep Water. *J. Phys. Oceanogr.*, **23**, 1885–1892.
- McCartney, M. S., 1993: The crossing of the equator by the deep western boundary current in the western Atlantic Ocean. *J. Phys. Oceanogr.*, **23**, 1953–1974.
- , and R. Curry, 1993: Trans-equatorial flow of Antarctic bottom water in the western Atlantic Ocean. *J. Phys. Oceanogr.*, **23**, 1264–1276.
- , S. L. Bennett, and M. E. Woodgate-Jones, 1991: Eastward flow through the Mid-Atlantic Ridge at 11°N and its influence on the abyss in the eastern basin. *J. Phys. Oceanogr.*, **21**, 1089–1120.
- Mercier, H., K. G. Speer, and J. Honnorez, 1994: Flow pathways of bottom water through the Romanche and Chain Fracture Zone. *Deep-Sea Res.*, **41**, 1457–1477.
- Metcalfe, W. G., B. C. Heezen, and M. C. Stalcup, 1964: The sill depth of the Mid-Atlantic Ridge in the equatorial region. *Deep-Sea Res.*, **11**, 1–10.
- Molinari, R. L., R. A. Fine, and E. Johns, 1992: The deep western boundary current in the tropical North Atlantic Ocean. *Deep-Sea Res.*, **39**, 1967–1984.
- National Geophysical Data Center, 1988: Digital relief of the surface of the Earth. Data Announcement 88-MGG-02, NOAA, Boulder, CO.
- Polzin, K. L., K. G. Speer, J. M. Toole, and R. W. Schmitt, 1996: Intense mixing of Antarctic bottom water in the equatorial Atlantic Ocean. *Nature*, **380**(6569), 54–57.
- Ponte, R. M., J. Luyten, and P. L. Richardson, 1990: Equatorial deep jets in the Atlantic Ocean. *Deep-Sea Res.*, **37**(4), 711–713.
- Rhein, M., L. Stramma, and U. Send, 1995: The Atlantic deep western boundary current: Water masses and transports near the equator. *J. Geophys. Res.*, **100** (C2), 2441–2457.
- , F. Schott, L. Stramma, J. Fischer, O. Plähn, and U. Send, 1996: The deep western boundary current in the tropical Atlantic: Deep water distribution and circulation off Brazil. *Int. WOCE Newsletter*, **23**, 11–14, 20.
- Speer, K. G., and W. Zenk, 1993: The flow of Antarctic Bottom Water into the Brazil Basin. *J. Phys. Oceanogr.*, **23**, 2667–2682.
- , —, G. Siedler, J. Pätzold, and C. Heidland, 1992: First resolution of flow through the Hunter Channel in the South Atlantic. *Earth Planet. Sci. Lett.*, **113**, 287–292.
- Tarbell, S. A., J. A. Whitehead, M. Hall, and M. S. McCartney, 1997: Trans-equatorial bottom water flow in the western Atlantic. Vol. XLVI (in a series of reports presenting data from moored current meters). Woods Hole Oceanographic Institution Tech. Rep. No. 9701, 86 pp. and 3 fiche. [Available from Woods Hole Oceanographic Institution, Woods Hole, MA 02543.]
- Whitehead, J. A., and L. V. Worthington, 1982: The flux and mixing rates of Antarctic Bottom Water within the North Atlantic. *J. Geophys. Res.*, **87**, 7903–7924.
- Wright, W. R., 1970: Northward transport of Antarctic Bottom Water in the western Atlantic Ocean. *Deep-Sea Res.*, **17**, 367–371.
- Wüst, G., 1957: Stromgeschwindigkeiten und Strommenger in den Tiefen des Atlantische Ozeans. *Wiss. Ergebn. dtsh. atlant. Expedition 'Meteor*, Bd. VI, 2. Teil, 6, 262–420.
- Zenk, W. and N. Hogg, 1996: Warming trend in Antarctic Bottom Water flowing into the Brazil Basin. *Deep-Sea Res.*, **43**(9), 1461–1473.